The lncRNA MIR31HG regulates the senescence associated secretory phenotype

Marta Montes (marta.montes@bric.ku.dk)
Biotech Research and Innovation Centre, University of Copenhagen
Michael Lubas
Biotech Research and Innovation Centre, University of Copenhagen
Frederic S Arendrup
Biotech Research and Innovation Centre, University of Copenhagen
Bettina Mentz
Biotech Research and Innovation Centre, University of Copenhagen
Neha Rohatgi
Genome Institute of Singapore, Agency for Science, Technology and Research (A*STAR)
Sarunas Tumas
Biotech Research and Innovation Centre, University of Copenhagen
Lea M Harder
Department of Biochemistry and Molecular Biology, University of Southern Denmark
Anders J Skanderup
Genome Institute of Singapore, Agency for Science, Technology and Research (A*STAR)
Jens S Andersen
Department of Biochemistry and Molecular Biology, University of Southern Denmark
Anders H Lund (anders.lund@bric.ku.dk)
University of Copenhagen https://orcid.org/0000-0002-7407-3398

Research Article

Keywords: Senescence, SASP, BRAF

DOI: https://doi.org/10.21203/rs.3.rs-57840/v1

Abstract

Senescent cells secrete cytokines, chemokines and growth factors collectively known as the senescence-associated secretory phenotype (SASP) which can reinforce senescence and activate the immune response. However, it can also negatively impact neighbouring tissues facilitating tumor progression. We have previously shown that in proliferating cells the nuclear long non-coding RNA (lncRNA) *MIR31HG* inhibits p16/CDKN2A expression through interaction with polycomb repressor complexes (PRC1/2) and that during BRAF-induced senescence *MIR31HG* is overexpressed and translocates to the cytoplasm. Here, we show that *MIR31HG* regulates the expression of a subset of SASP components during BRAF-induced senescence. The SASP secreted from senescent cells depleted for *MIR31HG* fails to induce paracrine invasion without affecting the growth inhibitory effect. Mechanistically, *MIR31HG* interacts with YBX1 facilitating its phosphorylation at serine 102 (p-YBX1^{S102}) by the kinase RSK. p-YBX1^{S102} induces *IL1A* translation which acts as upstream regulator inducing the transcription of the other SASP mRNAs. Our results suggest a dual role for *MIR31HG* in senescence depending on its cellular localization and points to the lncRNA as a potential therapeutic target in the treatment of senescence-related pathologies.

Introduction

Cellular senescence is an irreversible state of growth arrest that can be driven by several stimuli including telomere shortening due to extensive replication, DNA damage, oxidative stress or oncogene overexpression (Hayflick, 1965, Kuilman, Michaloglou et al., 2010). In addition, it has been recently shown that senescence can play a role in differentiation and tissue regeneration (Munoz-Espin, Canamero et al., 2013, Storer, Mas et al., 2013). Oncogene-induced senescence (OIS) was firstly reported by Serrano et al. when they observed that expressing an oncogenic form of Ras in primary fibroblast induced senescence (Serrano, Lin et al., 1997). Later work demonstrated that other oncogenes such as mutated BRAF promoted OIS both *in vivo* and *in vitro* (Braig, Lee et al., 2005, Michaloglou, Vredeveld et al., 2005). OIS has been considered as a barrier to prevent tumour progression and additional mutations in tumour suppressor genes are required in order to bypass senescence to promote malignancy (Braig et al., 2005, Chen, Trotman et al., 2005, Daniotti, Oggionni et al., 2004). Senescent cells show a characteristic morphology and biochemical features such as halted proliferation, enlarged size, activation of the senescence-associated b-galactosidase, expression of cell cycle inhibitors and the presence senescence-associated heterochromatin foci (SAHF). Importantly, in several types of senescence, the cells secrete factors such as interleukins, cytokines and metalloproteases, which are part of the senescence-associated secretory phenotype (SASP) that can impact the cellular environment and homeostasis of the neighbouring tissues (Acosta, Banito et al., 2013, Coppe, Patil et al., 2008, Kuilman, Michaloglou et al., 2008). The downstream effects of the SASP can be beneficial or detrimental depending on the tissue context (Coppe, Desprez et al., 2010, Salama, Sadaie et al., 2014). It has been shown to prevent cancer progression by reinforcing autocrine senescence, inducing paracrine senescence in neighbouring cells (Acosta et al., 2013, Kuilman et al., 2008), and by inducing tissue repair and regeneration (Demaria,

Ohtani et al., 2014, Munoz-Espin et al., 2013, Storer et al., 2013). The SASP can also activate the immune system facilitating the clearance of damaged cells (Iannello, Thompson et al., 2013, Xue, Zender et al., 2007). On the other hand, the SASP can promote tumorigenic processes such as angiogenesis and invasion (Coppe et al., 2008, Krtolica, Parrinello et al., 2001). During aging, excessive SASP secretion can induce chronic inflammation that can lead to aged-related pathologies (Baker, Wijshake et al., 2011, Jeyapalan, Ferreira et al., 2007). The composition of the SASP is very variable depending on different aspects such as the senescence stimuli and the cell type (Casella, Munk et al., 2019, Hernandez-Segura, de Jong et al., 2017). Defining the composition of the secretome and identifying new regulators in each biological context is crucial to identify molecular signatures of such a complex phenotype.

Previously, the lncRNA *TERRA* has been shown to be a component of inflammatory exosomes and to modulate transcription of inflammatory cytokines in recipient cells (Wang, Deng et al., 2015) and other lncRNAs have been reported to regulate NF-kB activation and its downstream target genes (Jin, Jia et al., 2016, Ozes, Miller et al., 2016, Rapicavoli, Qu et al., 2013). These findings raise the hypothesis that lncRNAs could act as key players in the SASP induction during senescence. A few lncRNAs have been directly linked to senescence (Li, van Breugel et al., 2018, Montes & Lund, 2016, Montes, Nielsen et al., 2015). We have previously identified the lncRNA *MIR31HG* to be upregulated in BRAF mediated OIS (Montes et al., 2015). In proliferating cells nuclear *MIR31HG* represses *p16/CDKN2A* expression by recruiting Polycomb group complexes. Indeed, we have shown that in melanoma patients harbouring BRAF mutations, *MIR31HG* negatively correlates with *p16/CDKN2A* expression (Montes et al., 2015). Upon BRAF induction *MIR31HG* is upregulated and translocates to the cytoplasm where we now show that it regulates the expression of a part of the SASP repertoire. *MIR31HG* knockdown in BRAF-induced senescent fibroblasts reduces expression and secretion of several components of the SASP. Interestingly, conditioned medium (CM) from *MIR31HG*-depleted senescent cells promotes paracrine senescence but fails to induce cancer cell invasion. Mechanistically, we show that *MIR31HG* promotes the interaction between YBX1 and the RSK kinase resulting in YBX1 phosphorylation and subsequent induction of IL1A translation. Our results unveil the role of lncRNAs in the regulation of the SASP highlighting the dual role in senescence of *MIR31HG* by suppressing CDKN2A expression in young cells and facilitating production of a distinct subset of SASP factors in senescent cells.

Results

MIR31HG knock-down decreases the induction of SASP components during senescence

To assess the role of *MIR31HG* during OIS we used immortalised human fibroblasts BJ-hTERT, expressing a constitutively active form of the mouse B-RAF (V600E) that is fused to the oestrogen receptor (BJ ER:BRAF). Addition of 1mM of 4-hydroxitamoxifen (4-OHT) activates BRAF inducing OIS (Pritchard, Samuels et al., 1995). We first confirmed that *MIR31HG* was overexpressed in BJ ER:BRAF upon 4-OHT induction (Figure 1A), as we previously reported for TIG3 ER:BRAF cells (Montes et al., 2015).

In validation of the model, analysis of TGCA data from thyroid and colorectal cancer tumor samples, where *BRAF* is frequently mutated, demonstrated a higher *MIR31HG* expression in tumors harbouring *BRAF* mutations (Figure 1B). We performed RNA sequencing in control cells and BRAF-induced senescent cells transfected with control siRNA or siRNA targeting *MIR31HG*. As expected, many genes were differentially expressed comparing control versus senescent cells (Figure 1C and Supplementary Table 1A and 1B). Moreover, the transcriptional profile of *MIR31HG* knock-down senescent cells resembled the senescent profile with several clusters of differentially expressed genes (Figure 1C and Supplementary Table 1A and 1B). Among the GO categories significantly represented among the genes specifically downregulated in the MIR31HG knock-down conditions we found cytokine and chemokine-related pathways (Supplementary Fig. 1A). Furthermore, we observed that senescent *MIR31HG*-depleted cells failed to upregulate part of the main SASP components previously defined (Coppe et al., 2010) (Figure 1D and Supplementary Table 1C and 1D). We validated transcriptomics data by RT-qPCR and confirmed that several interleukins and chemokines such as IL6 and CXCL1 were nearly absent at the RNA level, whereas other factors such as ICAM1 or IL1A were not affected (Figure 1E). To validate our results in another cellular system, we performed RT-qPCR analysis in TIG3 ER:BRAF cell line. Depletion of *MIR31HG* during BRAF induced senescence decreases the levels of the SASP RNAs (Supplementary Fig.1B). In order to analyse the composition of the SASP at the protein level, we knocked down *MIR31HG* in BJ ER:BRAF cells and induced senescence by 72-hour 4-OHT treatment in serum-free medium followed by mass spectrometry analysis of secreted proteins. Untreated cells transfected with control siRNA were used as control. As expected, control senescent cells, when compared to control proliferating cells, showed differential secretion of factors (Supplementary Fig.1C and Supplementary Table 2A and 2B). The secretome of senescent *MIR31HG* knock-down cells resembled that of control senescent cells with discrete differences (Figure 1F and Supplementary Fig. 1C and Supplementary Table 2A and 2B). Among the less secreted proteins upon *MIR31HG* depletion were inflammatory SASP factors IL6 and CXCL1 (Figure 1F, and Supplementary Fig.1D and 1E). The reduced secretion of these factors was validated by ELISA and western blotting using two different siRNAs for *MIR31HG* (Figure 1G and 1H). Altogether our results demonstrate that *MIR31HG* knock-down reduces the production of several SASP components during OIS already at the transcriptional level and these changes are reflected in the secretome.

The SASP of senescent *MIR31HG* knock-down cells induces senescence but not invasion in a non-autonomous manner

To determine the paracrine effect of the SASP we induced senescence in cells transfected with control siRNA or siRNAs targeting *MIR31HG*. After 72h 4-OHT treatment CM was harvested and used for subsequent analysis. The CM from proliferating cells without 4-OHT induction was also harvested at the same time point as control. To assess the potential of the SASP in inducing paracrine senescence, we incubated BJ WT cells with the different CM for 72h. Protein analysis of whole cell extracts by western blot revealed that BJ WT growing in CM from control senescent cells and *MIR31HG* knock-down senescent were both able to mildly upregulate the senescence marker p53 (Figure 2A) as well as the enzyme β-galactosidase (Figure 2B) compared to proliferating cells. However, the upregulation of inflammatory cytokines that occurs upon 4-OHT induction is reduced after *MIR31HG* depletion (Figure

2C). Acosta et al. reported that TGF-β signalling pathway is responsible for the paracrine senescence effect(Acosta et al., 2013). As expected, RNA levels of TGFβ target genes were upregulated in BJ ER:BRAF upon 4-OHT treatment compared to control proliferating cells (Supplementary Fig. 2A), while *MIR31HG* knock-down did not affect this increase. Moreover, the protein level of pSMAD2, downstream effector of TGFβ signalling, was upregulated during OIS in control as well as in *MIR31HG* knock-down senescent cells (Supplementary Fig. 2B). Similarly, WT BJ cells discretely activated TGFβ signalling when incubated with CM from control senescent cells and also with CM from *MIR31HG* knock-down senescent cells (Supplementary Fig. 2C and 2D). These results demonstrate that the TGFβ signalling pathway remains active in *MIR31HG* knock-down senescent cells suggesting that its activation could be responsible for the paracrine senescence induction. To determine the role of the SASP in promoting cancer cell invasion we performed transwell invasion assays using the different CM described above as chemoattractant in the lower chamber of the transwell for MDA-MB-231 breast cancer cells. After 48h incubation a higher number of MDA-MB-231 cells exposed to CM from senescent cells invaded through the matrigel membrane compared to proliferating CM (Figure 2D). In contrast, the CM of *MIR31HG* knock-down senescent cells did not promote invasion (Figure 2D). These results demonstrate that the paracrine senescence effect is retained in the SASP of *MIR31HG* knock-down senescent cells but not the induction of paracrine invasion. These findings suggest that the effect of *MIR31HG* in the SASP production does not occur at a general level but that only a subset of components is inhibited.

MIR31HG knock-down decreases CEBPB protein levels and NF-kB activation during OIS

As NF-kB and CEBPB regulate the expression of many SASP genes by stimulating their transcription (Acosta, O'Loghlen et al., 2008, Chien, Scuoppo et al., 2011, Kuilman et al., 2008) we investigated the possibility that *MIR31HG* knock-down affected the abundance or the activation of these transcription factors. As expected, the protein levels of CEBPB and activated phosphorylated RELA (p-RELA) (component of the NF-kB complex) increased during BRAF activation (Figure 3A). Interestingly, *MIR31HG* knock-down in senescent cells reduced CEBPB protein expression and activated p-RELA (Figure 3A) without affecting their mRNA levels (Supplementary Fig. 3A). In accordance, binding of CEBPB to the *IL6* promoter, a canonical CEBPB target, decreased significantly upon *MIR31HG* knock-down compare to control senescent conditions (Figure 3B). Consistently, NF-kB translocation to the nucleus was inhibited upon *MIR31HG* depletion (Figure 3C). Moreover, the signalling pathway upstream NF-kB activation was affected in *MIR31HG* knock-down senescent (Supplementary Fig. 3B). These results suggest that *MIR31HG* acts upstream of both CEBPB and NF-kB transcriptional activation.

MIR31HG knock-down decreases IL1A protein levels upon OIS induction

IL1A has been reported to function as an upstream regulator of the SASP (Orjalo, Bhaumik et al., 2009). In line with this, addition of human recombinant IL1A(hr-IL1A) in our model system induced expression of SASP components at the RNA level (Supplementary Fig. 3C). Blocking IL1A signalling using siRNA against IL1A reduced the levels of CEBPB expression upon senescence as well as the RNA levels of different components of the SASP (Supplementary Fig. 3D and 3E). Interestingly, while *IL1A* mRNA was

not affected by the levels of *MIR31HG* (Figure 1C), IL1A protein levels were strongly reduced in *MIR31HG* knock-down senescent cells compared to control senescent cells as measured by immunofluorescence staining (Figure 3D) and by western blotting of the total lysate (Figure 3E). Addition of human recombinant IL1A (hr-IL1A) rescued the incapacity of *MIR31HG* knock-down senescent cells to induce SASP RNA transcription (Figure 3F), IL6 secretion (Figure 3G) and NF-kB nuclear translocation (Supplementary Fig. 3F).

To test whether *MIR31HG* would be regulating IL1A at a translational level we performed polysome profiling in control senescent cells and senescent cells upon depletion of *MIR31HG*. The profiles obtained upon sucrose gradient separation in both conditions showed no major changes in polysome distribution (Figure 3H). Analysing the distribution of *IL1A* mRNA through the gradient we observed that the majority of the transcript present in the heavy polysome fractions (Figure 3I). Remarkably, a significant decrease of *IL1A* mRNA in these fractions was observed in *MIR31HG* knock-down senescent cells compared to control senescent cells (Figure 3J and Supplementary Fig. 3G). These results correlate with the decreased IL1A protein we observed upon these conditions. Distribution of *ACTB* mRNA through the gradient did not show any difference (Figure 3J and Supplementary Fig 3G). Despite the decrease in mRNA levels of other cytokines such as IL6, the similar distribution of their mRNAs through the gradient indicates an equal translation efficiency suggesting that the effect of *MIR31HG* on translation is specific for *IL1A* (Figure 3J and Supplementary Fig 3G). MTOR signalling has been recently involved in SASP regulation through IL1A signalling (Laberge, Sun et al., 2015). However, *MIR31HG* knock-down does not affect mTOR signalling activation (Supplementary Fig. 3H) indicating an alternative mechanism for *MIR31HG* regulation of IL1A. These findings suggest that *MIR31HG* is implicated in the modulation of the SASP by regulating the levels of IL1A independently of mTOR signalling pathway. HG

MIR31HG interacts with YBX1 and YBX1 knock-down phenocopies MIR31HG depletion

In order to elucidate the mechanism by which *MIR31HG* exerts its function in regulating the SASP, we purified endogenous *MIR31HG* with its associated proteins from UV-crosslinked senescent BJ ER:BRAF cells using antisense oligonucleotides containing locked nucleic acid (ASOs) complementary to the *MIR31HG* sequence coupled to magnetic beads (Figure 4A). Oligonucleotides against the RNA sequence of luciferase, not expressed in BJ ER:BRAF cells, were used as control. Mass spectrometry analysis of *MIR31HG*-associated proteins revealed a low number of significantly-enriched proteins among which several RNA-binding proteins (Figure 4B, Supplementary Table 2C and D). MIR31HG has been previously shown to interact with IκBα during osteogenic differentiation regulating NFκB activation(Jin et al., 2016). However, we did not detect IκBα in our pull-down experiments. The majority were heterogeneous nuclear ribonucleoproteins (hnRNPs) or other predominantly nuclear proteins, involved in RNA processing. Recent reports have demonstrated the role of PTBP1 in regulating the SASP composition through the regulation of the alternative splicing of genes implicated in intracellular trafficking (Georgilis, Klotz et al., 2018). However, since *MIR31HG* localizes mainly in the cytoplasm during OIS we focused on YBX1 as a protein with defined cytoplasmic functions (Figure 4B). YBX1 has been implicated in several cytoplasmic processes, such as translation or mRNA stability among others (Lyabin, Eliseeva et al., 2014). According

to previous findings, YBX1 prevents senescence in epidermal progenitors and knock-down of YBX1 induces senescence features in keratinocytes (Kwon, Todorova et al., 2018). Depletion of YBX1 had a minor impact on cell growth in untreated BJ ER:BRAF (Supplementary 4A and 4B). However, knock-down of YBX1 in BRAF-induced senescent cells mimicked *MIR31HG* knock-down phenotype. SASP components were decreased at RNA level in YBX1 knock-down senescent cells compared to control senescent cells (Figure 4C and 4D and Supplementary Table 3A and 3B). Likewise, reduction in the secretion of IL6 and CXCL1 upon YBX1 knock-down were comparable to the levels following *MIR31HG* knock-down (Figure 1E and 4E). Furthermore, IL1A protein levels were strongly reduced (Figure 4F) whereas the mRNA level remained unaltered (Figure 4D).

Formaldehyde crosslinked-RNA immunoprecipitation (RIP) of GFP-tagged YBX1 validated its interaction with *MIR31HG* (Figure 4G). As a positive control, we found YBX1 binding its own RNA as previously reported(Skabkina, Lyabin et al., 2005). Interestingly, YBX1 binds *IL1A* mRNA whereas other cytokines mRNAs are bound to a lesser extent (Figure 4G). Furthermore, no binding to abundant nuclear RNAs (*MALAT1*) or the mitochondrial RNAs previously used as negative controls(Matsumoto, Uchiumi et al., 2012) was identified.

Altogether, these results suggest that the interaction between *MIR31HG* and YBX1 might have a role in regulating the SASP during OIS by regulating IL1A translation. To study the biological function of the *MIR31HG* and YBX1 interaction we analysed the stability and localization of *MIR31HG* upon YBX1 KD, since stabilization of RNAs is a well-described function of cytoplasmic YBX1 (Evdokimova, Ruzanov et al., 2001, Yang, Wang et al., 2019). We did not observe changes in *MIR31HG* expression nor localization upon YBX1 knock-down (Supplementary Fig 4C and 4D). Moreover, protein levels of YBX1 did not change upon depletion of *MIR31HG* (Supplementary Fig 4E).

YBX1 is phosphorylated at serine 102 by RSK in BRAF-induced senescence

Several modifications which can affect YBX1 function have been reported (Prabhu, Hartley et al., 2015). Phosphorylation of serine in position 102 has been shown to be involved in the regulation of translation (Evdokimova, Ruzanov et al., 2006). We therefore studied the phosphorylation status of YBX1 and the putative implication of *MIR31HG* in YBX1 regulation. In order to analyse p-YBX1 in BRAF-induced senescence, we used an antibody that recognizes p-YBX1 at position S102 (p-YBX1^{S102}). Interestingly, we detected increased levels of this modification at different time points after BRAF induction (Figure 5A). Different kinases have been reported to be responsible for S102 phosphorylation such as AKT and RSK (Stratford, Fry et al., 2008, Sutherland, Kucab et al., 2005). We analysed the levels of activated AKT at different time points after 4-OHT induction and we observed that p-Akt decreased over time to nearly undetected levels already after 24h 4-OHT induction (Supplementary Fig 5A). The kinase RSK, however, is activated at early points during senescence induction and remain active at later time points (Figure 5B) suggesting that YBX1 might be a substrate for RSK during OIS. To investigate the role of RSK in YBX1 phosphorylation in BRAF-OIS, we treated the cells with specific RSK inhibitors. Treatment of senescent cells with the inhibitor FMK reduced the levels of p-YBX1^{S102} (Figure 5C). Moreover, BI-D780, a more

specific RSK inhibitor, was able to completely abolish phosphorylation of YBX1 in senescent cells (Figure 5C). Furthermore, overexpression of RSK resulted in an increased level of p-YBX1^{S102} (Supplementary Fig 5B). Our results conclude that YBX1 is phosphorylated by RSK kinase in a BRAF-dependent manner.

Phosphorylation of YBX1 at serine 102 induces translation of IL1A

It has been previously shown that YBX1 can promote translation of specific transcripts (El-Naggar, Veinotte et al., 2015, Evdokimova, Tognon et al., 2009). We next wondered whether p-YBX1^{S102} could impact *IL1A* translation. As expected, BRAF-induced senescence resulted in an upregulation of IL1A protein levels compared to control untreated cells (Figure 5D). Interestingly, treatment with the RSK inhibitor BI-D1780 failed to upregulate IL1A during senescence (Figure 5D). YBX1 has been recently implicated in cytokine translation by binding the 3'UTR of their mRNAs(Kwon et al., 2018). Using reporter plasmids harbouring the 3'UTR of IL1A after luciferase gene we demonstrated that a WT version of YBX1 is able to increase luciferase translation in response to 4-OHT induction. A mutant that is not able to be phosphorylated at S102 (S102A) failed to induce translation whereas a phosphomimic mutant (S102D) increased translation even in the absence of 4-OHT (Figure 5E and Supplementary Fig. 5D). These results suggest that p-YBX1 binds *IL1A* 3'UTR to increase its translation. We assessed the binding capacity of the different phosphorylated versions of YBX1 to *IL1A* mRNA and to *MIR31HG* by RIP. All the proteins showed a similar binding to their targets suggesting that phosphorylation at S102 is not affecting YBX1 binding capacity (Figure 5F).

MIR31HG knock-down in senescent cells reduces cytoplasmic p-YBX1 inhibiting its interaction with RSK

We next examined whether *MIR31HG* might have an impact on YBX1 phosphorylation. We performed cellular fractionation to analyse the localization of phosphorylated YBX1 in senescent cells and in senescent cells where *MIR31HG* was depleted. Interestingly, we observed that upon *MIR31HG* knock-down p-YBX1 is reduced in the cytoplasm (Figure 6A and Supplementary Fig. 6A) suggesting a role for MIR31HG in the phosphorylation process of YBX1. Several cytoplasmic lncRNAs have been shown to act as scaffolds for bringing molecules into close proximity. In order to analyse whether MIR31HG was binding both YBX1 and its kinase RSK, we performed native RIP using GFP-tagged version of RSK. We could not detect RSK binding to *MIR31HG* (Supplementary Fig. 6B and 6C). To further analyse the role of *MIR31HG* in the interaction of YBX1 with its kinase RSK, we performed proximity ligation assays (PLA) using antibodies against total YBX1 and total RSK. Importantly, the interaction was higher in senescence compared to control (Figure 6B). Interestingly, *MIR31HG* knock-down reduced the level of interaction confirming our hypothesis that *MIR31HG* mediates YBX1 interaction with its kinase RSK during OIS (Figure 6B).

Discussion

The SASP is a hallmark of senescent cells and responsible for mediating the patho-physiological effects in the surrounding tissues. For a long time, efforts in the field have been focused on trying to induce senescence in cancer cells in order to prevent cancer progression (Braig et al., 2005, Ventura, Kirsch et al., 2007, Wu, van Riggelen et al., 2007). In contrast hereto, more recent reports have shown that targeting senescent cells strongly improve age-related diseases (Baker et al., 2011, Farr, Xu et al., 2017, Xu, Palmer et al., 2015). Although recent work has extended our knowledge of the signalling network upstream the transcriptional induction of the SASP components (Freund, Patil et al., 2011, Herranz, Gallage et al., 2015, Hoare, Ito et al., 2016, Kang, Xu et al., 2015, Tasdemir, Banito et al., 2016), the complexity and diversity of the SASP suggest that additional regulators might be involved. It is crucial to acquire further knowledge of the detailed mechanism to be able to design therapies for cancer, inflammation and aging treatment. Here, we contribute to understanding the SASP regulation by describing the molecular mechanism by which the lncRNA *MIR31HG* regulates a subset of the SASP components during BRAF-induced senescence by modulating *IL1A* translation. It is known that most of the SASP components are regulated at the transcriptional level, although a small fraction may additionally be regulated by post-transcriptional mechanisms (Herranz et al., 2015, Laberge et al., 2015). In this study, we focus on the senescence process initiated following the expression of a mutated *BRAF*. This is of importance as somatic mutations in *BRAF* occur in approximately 7% of human cancer (Davies, Bignell et al., 2002). We observed that *MIR31HG* expression is higher in thyroid and colorectal cancer tumor samples harbouring *BRAF* mutations, as compared to *BRAF* wild type, suggesting the relevance of this lncRNA in cancer.

We find that the secretome from BJ ER:BRAF senescent cells and BJ ER:BRAF *MIR31HG* knock-down senescent cells show differences in the levels of key SASP components. Whereas most of the genes deregulated at transcription level are also altered at the protein level, a small proportion is regulated only at RNA or protein level. This, together with the comparable polysome distribution profiles of these cell lines, suggest no changes in global translation upon *MIR31HG* depletion. Interestingly, IL1A, an upstream regulator of the SASP, is reduced at the protein level following *MIR31HG* knock-down whereas the mRNA level is not significantly altered. No IL1A was detected in the conditioned media by mass spectrometry or by ELISA (data not shown), likely due to the fact that IL1A remains attached to the membrane during OIS as previously described (Orjalo et al., 2009). In our cellular system addition of hr-IL1A induces the transcription of several cytokines and instigates the SASP. Intriguingly, it also rescues the decreased transcription of SASP components caused by *MIR31HG* depletion during BRAF-induced senescence. These results strongly support the idea of *MIR31HG* regulating IL1A as an upstream regulator of the SASP transcriptional program. Work from the Campisi lab has demonstrated that the translation of *IL1A* during RAS-induced senescence is regulated by mTOR (Laberge et al., 2015). Although the mTOR pathway is increased in our OIS model, it is not altered in *MIR31HG* knock-down conditions. Instead, we found the lncRNA *MIR31HG* to affect *IL1A* translation through YBX1. Endogenous *MIR31HG* pull-down and subsequent validations by RIP show that YBX1 is a *MIR31HG* binding partner. Importantly, YBX1 depletion mimics the *MIR31HG* knock-down phenotype in BRAF-induced senescence. This includes the reduced translation of *IL1A* and therefore the downregulation of downstream SASP components at RNA level, such as CXCL1, IL8 or IL6 among others. Interestingly, recent work has shown that YBX1 prevents

cytokine translation in cycling keratinocytes by binding their 3'UTR. In these studies, YBX1 knock-down results in increased translation of several cytokines and therefore induction of senescence (Kwon et al., 2018). In proliferating BJ cells, knock-down of YBX1 does induce a slight decrease of cell growth consistent with this report. However, knock-down of YBX1 in cells subjected to BRAF-induced senescence resulted in reduced RNA levels of most of the cytokines previously annotated as SASP components (Coppe et al., 2010). Interestingly, in BRAF-induced senescence we observe that YBX1 binds a high fraction of the IL1A mRNA while binding other cytokines to a lesser extent. YBX1 binds AU-rich motifs present in the 3'UTR of cytokine mRNAs (Beiter, Hoene et al., 2015, Kwon et al., 2018), which is consistent with our *IL1A* 3' UTR luciferase reporter assays. However, the stronger binding of YBX1 to *IL1A* mRNA compared to other cytokines show some degree of specificity towards *IL1A* mRNA. The mechanism underlying this specificity remains unknown. In a recent study, Dominguez and colleagues determined the importance of contextual features in RNA recognition by RBPs (Dominguez, Freese et al., 2018). Perhaps RNA secondary structures, the flanking nucleotide composition or the proximity to other RNA-binding proteins might be influencing the binding of YBX1 to the *IL1A* mRNA.

We observe an increase in p-YBX1^{S102} in BRAF-induced senescence and, importantly, p-YBX1^{S102} is reduced in the cytoplasm upon *MIR31HG* knock-down. Our results indicate that this post-transcriptional modification of YBX1 is involved in promoting *IL1A* translation during BRAF-induced senescence through its 3'UTR, which could explain the previously reported opposite roles of YBX1 in cytokine translation(Kwon et al., 2018). The role of p-YBX1 in translation remains to be fully understood. It is known that YBX1 binds the mRNA cap structure by displacing the eukaryotic translation factor 4E (eIF4A) and eIF4G and hence promotes translational repression (Evdokimova et al., 2001, Nekrasov, Ivshina et al., 2003). p-YBX1^{S102} on the other hand binds the mRNA cap structure less tightly allowing translation of repressed mRNAs (Evdokimova et al., 2006). However, not much is known about its role in promoting translation. Our luciferase reporter assay indicates that during senescence, p-YBX1^{102} may have a role in promoting *IL1A* translation through the 3'UTR since the phosphomutant YBX1^{S102A} fails to induce luciferase induction. Mutation of S102 did not alter YBX1 binding capability to *IL1A* or other mRNAs, consistently with previous reports demonstrating that phosphorylation at S102 does not affect the general RNA binding capacity of YBX1 (Evdokimova et al., 2001) . Phosphorylation of translation factors are determining events occurring during translation regulation (Proud, 2019) and perhaps p-YBX1 is involved in differentially recruiting other translation factors with a role in *IL1A* mRNA translational regulation. Further phospho-proteomic studies would help to address this question. We cannot exclude that phosphorylation at other residues occur during senescence. In fact, S165 and S176 has been shown to activate NF-kB signalling (Martin, Hua et al., 2017, Prabhu, Mundade et al., 2015). It would be interesting to investigate whether these modifications have any impact in senescence or in translation regulation.

LncRNAs can modulate post-transcriptional modifications of proteins (Li, Liu et al., 2017, Lo Piccolo, Mochizuki et al., 2019, Wang, Xue et al., 2014, Yoon, Abdelmohsen et al., 2013). Our results suggest that during BRAF-induce senescence RSK appears to be the main kinase responsible for YBX1

phosphorylation. PLA experiments show an increase in RSK-YBX1 interaction during OIS correlating with an increased level of p-YBX1. Despite at a lower level, the presence of interaction in proliferating conditions suggests that the interaction may occur without BRAF induction. The signalling cascade activated during OIS might be necessary to phosphorylate YBX1 at least at S102. We cannot exclude that RSK phosphorylates other residues in proliferating cells. Nevertheless, our results indicate that MIR3HG is important for the YBX-RSK interaction during senescence, when the lncRNA is expressed and predominantly located in the cytoplasm (Montes et al., 2015). We do not detect *MIR31HG* directly binding RSK, likely excluding a role for *MIR31HG* as scaffold bridging together YBX1 and its kinase. Instead, *MIR31HG* interaction with YBX1 might infer an optimal conformation to facilitate its phosphorylation. Another possibility is that the interaction between YBX1 and *MIR31HG* brings YBX1 to another protein or protein complex required for the phosphorylation. Structural studies or more exhaustive phospho-proteomic analysis could improve our understanding on how *MIR31HG* promotes YBX1 phosphorylation under OIS.

The SASP has been reported to either limit or promote tumor progression. Dissociation of the good and bad sides of the SASPs is difficult since many of its components can have both roles depending on the cellular context (Salama et al., 2014). Besides, many of the senescence effectors are activated by the same pathways that activate the SASP. Therefore, the identification of factors that can affect the SASP without altering the tumour-suppressive effects associated with senescence is a promising strategy for senescence-related therapies. Several reports have described factors that can uncouple the senescence growth arrest from the SASP (Georgilis et al., 2018, Herranz et al., 2015, Laberge et al., 2015, Tasdemir et al., 2016). Here, we identify a lncRNA that, when located in the cytoplasm during OIS, is responsible for the production of a distinct subset of SASP components. Its depletion during OIS leads to a decrease of interleukins, chemokines and other factors preventing invasion *in vitro* without reverting growth arrest. Interestingly, we have previously described a mechanism for the nuclear *MIR31HG* in proliferating cells in repressing $p16^{INK4A}$ expression by recruiting polycomb group proteins (Montes et al., 2015). Altogether, our results suggest that the lncRNA *MIR31HG* has a dual role in inducing and buffering senescence depending on the cellular localization, which highlights the complexity of the regulation of senescence and the SASP. Interestingly, *MIR31HG* has been reported to be upregulated in different types of cancer (Eide, Eilertsen et al., 2019, Shih, Chiang et al., 2017, Yang, Liu et al., 2016). The fact that depletion of *MIR31HG* induces p16 expression without activation a SASP response (Montes et al., 2015) and decreases pro-invasive factors during SASP induction makes it an interesting target for therapeutic purposes. Inhibition of *MIR31HG* as well as other anti-SASP therapies could be potentially used to ameliorate the detrimental effects of senescence cells.

Materials And Methods

Cell lines

The human diploid fibroblast cell lines TIG3 (lung) and BJ (foreskin) were immortalized with telomerase (hTERT) and transduced with a retrovirus generated from pMSCV-ER:B-RAF as previously described

(Christoffersen, Shalgi et al., 2010). BJ ER:BRAF, TIG3:BRAF, BJ wild type (WT) and MDA-MB-231 cells were maintained in Dulbecco's modified Eagle's medium (Invitrogen) supplemented with 10% FBS (Hyclone) and penicillin/streptomycin (Invitrogen).

Treatments and siRNA transfections

Senescence was induced by treatment with 1μM 4-hydroxytamoxifen (4-OHT, Sigma) 24h after cell seeding for at least 48h (unless otherwise indicated). siRNA oligonucleotides were transfected at a final concentration of 50nM by reverse transfection using RNAiMAX (Invitrogen) according to the manufacturer's instructions for 48h or 72h. In case of senescence induction, 1μM 4-OHT was added 24h after transfection to fresh media for 48h for RNA analysis or 72h for protein analysis. Primer sequences are listed in Supplementary Table 4. BI-D1780 (Axon 1528) and FMK (Gift from Morten Frodin) Rsk inhibitors were used at 10uM for the time indicated in each experiment.

MIR31HG expression analysis in tumor samples

Gene expression (RNAseq) and somatic mutation data for tumors in The Cancer Genome Atlas (TCGA Pan-Cancer) were downloaded from UCSC Xena platform(Goldman, Craft et al., 2019). Thyroid carcinoma (THCA) and colo-rectal adenocarcinoma (COAD & READ) were used for analysis because these tumors have high frequency of BRAF mutations (>10%) and also express MIR31HG. Expression values for all the samples were converted to log2(fpkm+1) unit. Wilcoxon test was performed to compare the expression differences in the BRAF mutant and BRAF wild type tumors, using R.

YBX1-GFP and RSK-GFP overexpressing cell lines

To generate lentiviral constructs, we cloned the coding sequence of YBX1 amplified from cDNA, into the inducible vector pLVX-TetOne Puro Vector (Clontech) that already contained GFP-fusion protein. We use In-Fusion HD Cloning designing primers according to the manufacturer’s indications.

For the lentiviral production, HEK293T cells were transfected using lipofectamine 2000 (Lifetechnologies) with 7μg of pLVX-YBX1-GFP or pLVX-empty-GFP, together with 6μg of VsVg and 5μg Pax8 viral plasmids. After 48h supernatants containing the viral particles were filter through a 0.45μm filter. Confluent BJ ER:BRAF cells were then transduced with 1/3 of the viral supernatant and 8 μg/μl polybrene. 24h post-transduction the cells were selected with 1 μg/ul puromycin. Cells were maintained in tetracycline-free tested serum (Clontech). For the expression of YBX1, 100ng/ml doxycycline was used for 72h unless otherwise indicated.

To generate the phosphomutant (S102A) and phosphomimic (S102D) versions of the protein, directed mutagenesis was performed using QuikChange II XL Site-Directed Mutagenesis Kit (Agilent) directly from the pLVX-YBX1-GFP construct. Primers with the respective mutations were designed according to the manufacturer’s indications. The pLVX-RSK-GFP cell line was generated as described for YBX1, amplifying the coding sequence from cDNA with specific primers. Primer sequences are listed in Supplementary Table 4.

RNA extraction and qRT-PCR analysis

Total RNA was isolated using Trizol reagent (Invitrogen), treated with TURBO DNase (Ambion, Lifetechnologies) and reverse transcribed using TaqMan Reverse Transcription kit (Applied Biosystems) with random hexamer primers. Quantitative real-time PCRs were performed using Syber Green PCR Fast PCR Master Mix 2x (Applied Biosystems). The housekeeping genes HPRT1 and RPLP0 were used for normalization of qRT-PCR data, unless otherwise stated. Primer sequences are listed in Supplementary Table 4.

Western blot analysis

Cells were seeded and reverse transfected in 6-well plates (NUNC). In case of senescence, cells were treated the following day with 1 μM 4-OHT. After 72h cells were harvested, washed once with PBS and the pellets lysed in RIPA buffer (150 nM NaCl, 0.1% sodium deoxycholate, 0.1% sodium dodecyl sulfate, 50 mm Tris–HCl (pH 8), 1 mM EDTA) containing protease inhibitors (Complete Mini Protease Inhibitor Cocktail; Roche Applied Science). Proteins were separated by electrophoresis in 4–12% NuPAGE Bis–Tris gels (Invitrogen) and transferred to nitrocellulose membranes (Amersham). Antibodies used are listed in Supplementary Table 5.

Conditioned media

To generate conditioned media the cells transfected and treated as indicated were growing in serum-free growth media for 24h. The media was filtered through a 0.45uM filter, centrifuged at 500g for 5min and placed on the corresponding recipient cells for the time indicated in each experiment.

Enzyme-linked immunosorbent assay (ELISA)

To measure the secretion of IL6 and CXCL1 the CM from different conditions were analysed by ELISA using commercially available kits (Thermo Fisher Scientific).

Secretome analysis

The CM for proteomics analysis was harvested from 6 cm plates as indicated above. CM was concentrated using Centricon (Milipore) 3kDa filter, precipitated by TCA and washed in acetone. Protein pellets were resuspended in 6M GndHCl in 10mM Tris/HCl pH 8.0 with 2mM DTT and incubated at 56°C for 30min. In-solution digestion was performed after sample dilution with 50mM TEAB using 250ng of LysC (Wako) (at 2M GndHCl) and followed by 500ng of trypsin (Promega) (at 0.6M GndHCl). Reduced, alkylated and acidified peptides were desalted on 100ul C18 stage tips (Thermo) and subjected to LC-MS/MS analysis.

Tryptic peptides were identified by LC-MS using an EASY-nLC 1000 (ThermoFisher Scientific) coupled to a Q Exactive HF (ThermoFisher Scientific) equipped with a nanoelectrospray ion source. Peptides were separated on an in-house packed column of ReproSil-Pur C18-AQ, 3μm resin (Dr Maisch, GmbH) using a

90-minute gradient of solvent A (0.5% acetic acid) and solvent B (80% acetonitrile in 0.5% acetic acid) and a flow of 250 nL/min. The mass spectrometer was operated in positive ion mode with a top 12 data-dependent acquisition, a resolution of 60,000 (at 400 m/z), a scan range of 300 – 1700 m/z and an AGC target of 3e6 for the MS survey. MS/MS was performed at a scan range of 200-2000 m/z using a resolution of 30,000 (at 400 m/z), an AGC target of 1e5, an intensity threshold of 1.0e5 and an isolation window of 1.2 m/z. Further parameters included an exclusion time of 45 sec and a maximum injection time for survey and MS/MS of 15 ms and 45 ms respectively.

The raw files obtained from LC-MS were processed using the MaxQuant software 72 version 1.5.3.30. Peak lists were searched against the human UniProt database using the Andromeda search engine incorporated in MaxQuant with a tolerance level of 7 ppm for MS and 20 ppm for MS/MS (Cox & Mann, 2008). Trypsin was chosen as digestion enzyme with max 2 missed cleavages allowed. Variable modifications were set to methionine oxidation, protein N-terminal acetylation, deamidation of asparagine and glutamine. Carbamidomethylation of cysteine was set as fixed modification and other parameters were kept as default.

Statistical analysis was conducted in R environment (https://www.r-project.org) using DEP (v. 1.8.0) bioconductor package for proteomics analysis, and visualizations were made using the ggplot2 R package(Wickham, 2016). Imputation of missing data was performed using MinProb setting based on minimal intensity values observed for each sample.

Crystal violet staining

Cells were seeded and reverse transfected in 6-well or 12-well plates (NUNC). 24, 48 and 72h after transfection or treatment cells were washed twice in PBS and fixed with 10% formalin for 10 min and stained with 0.1% crystal violet solution for 30 min. Excess crystal violet stain was removed by several washes with water. The plates were allowed to dry and crystal violet was extracted by the addition of 10% acetic acid. The amount of crystal violet staining was quantified by measurement of the absorbance at 570 nm.

Senescence associated β-galactosidase staining

Cells were seeded and transfected in 12-well plates (NUNC). At 72h post-transfection they were fixed and stained using the β-galactosidase staining kit (Cell signaling) according to the manufacturer's protocol.

Invasion assay

50 ul of 0.5ug/ml Matrigel LDEV-Free (Corning)was added to the transwell. 400ul of the desired CM was placed at the bottom of the transwell with 8.0 µm pore size (Croning). 50.000 MDA/MB-231 cells were resuspended in 200ul DMEM without FBS and place on top of the transwell. After 48h cells across the matrigel membrane were washed in PBS and fixed in cold 70% ethanol for 15 mins and stained using crystal violet staining as indicated above.

Cell fractionation

Cells were grown in 15 cm dishes (Nunc). Nuclear/cytoplasmic fractionation was performed using Nuclei EZ Lysis Buffer (Sigma) following the manufacturer's protocol.

Immunofluorescence

Cells were seeded on multichamber slides (Nunc) and transfected or treated. 72h cells were washed with PBS 1x and fixed in 4% paraformaldehyde (PFA) (Sigma) for 15 min. The cells were permeabilized by incubation with 0.1% Triton X-100 in PBS (Sigma) for 10min and blocked for 30 min with 5% normal goat serum in PBS before incubation with the primary antibodies in 2% normal goat serum overnight. After intensive washing with PBS 1x, the secondary antibody was incubated in 2% goat serum for 1h at room temperature in the dark. The coverslips were washed, drained and mounted on glass slides using Prolong Gold Antifade Reagent with DAPI (ThermoFisher Scientific). Images were taken using a Zeiss fluorescence microscope.

Chromatin Immunoprecipitation

Cells were fixed with 1% formaldehyde for 10 min. Crosslinking was arrested by adding glycine (0.125 M) for 5 min at room temperature. The cells were subsequently harvested in SDS lysis buffer (0.5% SDS, 100mM NaCl, 50mM Tris-Cl pH8.1, 5mM EDTA pH 8.0, protease inhibitor mixture Complete [Roche], and 1 mM phenylmethylsulfonyl fluoride [PMSF]. Nuclei were pelleted and resuspended in IP buffer (2volumes SDS lysis buffer:1 volume Triton-X buffer [100mM Tris-Cl, pH 8.6, 100mM NaCl, 5mM EDTA pH 8.0, 5% Triton X-100]). The lysates were sonicated using BIORUPTOR sonicator for 12 cycles of 30sec and centrifuged at maximum speed. The sheared chromatin was diluted to 1ml with IP buffer and precleared with salmon sperm DNA/recombinant protein A-agarose (ThermoFisher Scientific) for 2 h. 1% of the sample was used as the input control, and the remaining precleared chromatin was incubated overnight with 10 µg of antibody by incubation with salmon sperm DNA/protein-A agarose (50% slurry) and centrifugation. The bead pellets were washed in low or high salt conditions (0.1% SDS, 1% Triton X-100, 2 mM EDTA pH 8.0, 20 mM Tris-HCl pH 8.0, and 150 mM [low]/500 mM [high] NaCl). The beads were then washed once with LiCl buffer (0.25 M LiCl, 1% NP-40, 1% Na-deoxycholate, 1 mM EDTA, and 10 mM Tris-HCl pH 8.0) followed by two washes with Tris-EDTA buffer. Elution buffer (0.1% SDS, 0.1 M $NaHCO_3$) was added to the samples and the crosslinking was reverted by incubation at 68°C overnight. Samples were incubated 1h at 37°C with RNAse A (Sigma) and 45 min at 50°C with proteinase K (Ambion). The DNA was purified using Minelute PCR Purification Kit (Qiagen) and then amplified by qPCR. Primer sequences are listed in Supplementary Table 4.

RNA sequencing and bioinformatic analysis

RNA integrity was confirmed on Agilent 2100 Bioanalyzer using Agilent RNA 6000 Nano kit (Agilent Technologies). RNA-seq libraries were prepared from 2 µg total RNA with CATS mRNA-seq Kit (with polyA selection) v2 x24 (Diagenode) according to the manufacturer's protocol. Concentrations of the libraries

were measured using the Qubit fluorometer (Invitrogen) and fragment size was assessed on Agilent 2100 Bioanalyzer using Agilent High Sensitivity DNA kit (Agilent Technologies). The libraries were sequenced on Illumina NextSeq500 with 75 bp single-end. Raw reads were trimmed using Cutadapt (Martin, 2011) to remove adapters and minimum read length after trimming was set to 18. Trimmed reads were mapped to hg38 using STAR aligner(Dobin, Davis et al., 2013) (version 2.5.1a). Uniquely mapped reads were counted towards genes using featureCounts(Liao, Smyth et al., 2014) (version 1.5.1). Differential expression analysis was performed with DESeq2(Love, Huber et al., 2014) using FDR < 0.01. Heatmaps were generated using pheatmap package in R with default settings and relative expression as RPM calculated by Z-score scaling. GO-term analysis was carried out using PANTHER(Thomas, Campbell et al., 2003) (http://pantherdb.org/about.jsp, version 14.1) using Fischer's exact test with FDR multiple test correction. Only genes differentially expressed between Senescence and Senescence MIR31HG-KD and $|\log_2 \text{fold-change}| > 0.75$ were used for GO-term analysis.

MIR31HG oligonucleotide-based pull down

Cells were grown in 150 and 500 cm2 dishes in 25 or 90ml media respectively up to ~90% confluency. Prior to collection cell were irradiated with UV light at 254 nm, then scraped in ice-cold PBS, spun down at 800 x g for 5min at 4°C and stored at -80°C. Amino-C12-LNA-containing oligonucleotides against MIR31HG and luciferase (five per target, Exiqon, custom design) were coupled to Dynabeads MyOne Carboxylic Acid (Thermo Fisher Scientific) according to the manufacturer instructions using 1.5nmol oligo per 100ul beads. Prior to use, the coated beads were blocked in RNA pulldown (RP) buffer (50mM Tris/HCl ph7.5, 5mM EDTA, 500mM LiCl, 0.5% DDM, 0.2% SDS, 0.1% Na-deoxycholate, 4M Urea, 2.5M TCEP, protease inhibitors (Roche)) with addition of ssDNA (200ug/mL) and BSA (1mg/mL) and yeast RNA (200ug/mL). 0.5g cell pellet was used per condition and resuspended in 5mL volume of RP buffer with murine RNase inhibitor (NEB, 1:500). Lysates were sonicated in 15mL tubes with Branson tip sonicator (2x 10sek, with 30sek break, at setting 15%) and clarified at 16000 x g for 5min at 4°C. Supernatants were transferred to 2mL tubes and pre-heated to 65°C with 1200rpm shaking, then oligonucleotide-coated beads were added to lysates for 4h incubation at 65°C with shaking (250ul beads/0.5g initial cell pellet distributed in 2ml tubes). The beads were washed four times with RP buffer at room temperature and then washed with 1mL 50mM TEAB buffer to remove detergents. For mass spectrometry sample preparation the beads were resuspend in 100ul 50mM TEAB buffer (Sigma) including 2mM DTT. Trypsin was added (500ng) for O/N incubation at 37°C, then followed by treatments with DTT (10mM) and IAA (55mM) and acidification with TFA. 100ul StageTips (Thermo Fisher Scienfic) were used for desalting and purified peptides were subjected to LC-MS analysis (as described in the above section).

Samples were analyzed using instrument settings described above, and the obtained data was analyzed with MaxQuant v. 1.5.2.8, using N-terminal acetylation and methionine oxidation as variable modifications. Fold change values of median peptide intensities were calculated for 5 replicates, and missing values were imputed using minimal intensity value detected in the analysis. Significantly enriched proteins in MIR31HG pulldown samples over control pulldown were selected based on pvalue <

0.05, signal intensity (fold enrichment over luciferase control) and number of unique peptides present in majority of replicates.

Polysome Profiling

Prior to harvesting, cells were treated with 100 µg/mL cycloheximide (Sigma-Aldrich) for 3 min. Cells were washed and scrapped off in ice-cold PBS containing 100 µg/mL cycloheximide. Cell were lysed in excess of polysome lysis buffer (20 mM Tris-HCl, 150 mM KCl, 5mM MgCl2, 0.5% NP40 (Igepal CA-630, Sigma-Aldrich), 2 mM DTT, 100 µg/mL cycloheximide, Roche EDTA-free Protease Inhibitor (Roche) and murine RNase inhibitor (NEB)) and incubated while rotating for 10 min at 4ºC. Debris, nuclei and mitochondria were cleared by centrifugation at 12.000g for 15 min at 4ºC. Lysate material was normalized to equal A_{260} value measured on NanoDrop. Normalized lysate, 400 µL total, was loaded on top of a 7% - 47% (w/v) linear sucrose gradient (Sigma) in open top polyallomer tubes (Seton Scientific) and centrifuged at 38.000g for 2.5 h at 4^{o} C using a Beckman ultracentrifuge (Optima L-90K, Class S) with the SW40ti rotor head (Beckman). Following ultracentrifugation, gradients were fractionated by piercing the tube bottom (Brandel Piercer), pushing gradient with 60% sucrose solution at a pace of 1 mL per minute while continuously measuring A_{260} using BioLogicP system (BioRad). RNA was subsequently extracted from each fraction by QIAzol (Qiagen) and chloroform extraction. Prior to RNA extraction, 20 pg of firefly-luciferase in vitro transcribed RNA was spiked into each fraction to control for potential loss of material in extraction protocol.

Luciferase reporter assays

For the luciferase reporter assays the 3'UTR of IL1A was cloned amplified by PCR from cDNA (see primer list). The PCR constructs were cloned into the pGL3-promoter Firefly luciferase reporter vector (Promega) using XbaI restriction enzyme.. 40.000 YBX1-GFP cells were reverse transfected with siRNAs against endogenous YBX1 in a 24-well plate. After 24h the cells were transfected using Lipofectamine 3000 (Lifetechnologies) with 500ng of the PGL3-promoter or PGL-3_IL1A-3'UTR together with 150ng of pRL-Tk Renilla luciferase reporter vector for transfection control and luciferase assay normalization. 24 hours after transfection fresh media containing 1µM 4-OHT was added to the cells. 48h after treatment Firefly and Renilla luciferase units were measured using Dual-Glo Luciferase Assay System and GLo-Max Multi Detection System (Promega).

Proximity ligation assay (PLA)

Cells were reverse transfected and seeded in 8-well multichamber slides (Nunc® Lab-Tek® II Chamber Slide™ system). 24h later media was changed and 1µM 4-OHT was added to the corresponding wells. After 72h cells were fixed in 4% formaldehyde for 15minutes and processed for PLA using Duolink® In Situ Orange Starter Kit Mouse/Rabbit (Sigma) according to manufacturer instructions. Images were

obtained using fluorescence microscope (Zeiss) and quantified using Cell Pofiler software. 5-10 images were quantified from 4 independent experiments.

Formaldehyde crosslinked RNA immunoprecipitation (RIP)

Cells were seeded in 15cm plates and treated with 1µM 4-OHT the day after for 48 hours. The cells were washed twice with PBS and crosslinked with 1% formaldehyde in PBS shaking for 15 minutes. Crosslinking was stopped incubating with glycine 0.25M for 5 minutes. After extensive washing with cold PBS the cells were centrifuged at 800g for 5 minutes. 80-100 mg of cell pellet was resuspended in lysis buffer (50mM TRIS/HCl, pH 7.4, 100mM NaCl, 0.5% Triton X-100, 5mM EDTA, 0.25% Na-deoxycholate, Protease Inhibitor (Roche), RNase Inhibitor (NEB)) and sonicated 3 cycles of 10 sec using a BRANSON sonicator at setting 15%. After 15 minutes centrifugation at 16000g the supernatant was collected in a new tube. 10% of the extract was saved as RNA input. The rest of the cell extract was incubated with 10ul of GFP-Trap® Magnetic Agarose beads (Chromotek) rotating at 4°C for 2 hours. The beads were then collected using a magnetic rack and washed once with lysis buffer and 5 times with high salt buffer ((50mM TRIS/HC pH 7.4, 1000mM NaCl, 0.5% Triton-X100, 1M Urea, 5mM EDTA, 1mM DTT). After the last wash, the beads were resuspended in 100 ul of RIP buffer (50mM Hepes pH. 7.5, 0.1M NaCl, 5mM EDTA, 10mM DTT, 0.5% TritonX100, 1% SDS) and incubate 45 minutes at 70°C to revert crosslinking. Proteins were digested incubating for 20 minutes at 37°Cwith 10ul proteinase K (Invitrogen, ThermoFisher). RNA was extracted adding 600ul of TRIzol reagent (Invitrogen, ThermoFisher) using manufacturers protocol.

Native RNA immunoprecipitation

Cells were seeded in 15cm plates and treated with 1µM 4-OHT the day after for 48 hours. The cells were washed twice with PBS and centrifuged at 500g for 5 minutes. The pellet was resuspended in lysis buffer (50mM TRIS/HCl, pH 7.4, 100mM NaCl, 0.5% Triton X-100, 5mM EDTA, 0.25% Na-deoxycholate, Protease Inhibitor (Roche), RNase Inhibitor (NEB)). After 15 minutes centrifugation at 16000g the supernatant was collected in a new tube. 10% of the extract was saved as RNA input. The rest of the cell extract was incubated with 10ul of GFP-Trap® Magnetic Agarose beads (Chromotek) rotating at 4°C for 2 hours. The beads were then collected using a magnetic rack and washed three times with lysis buffer. RNA was extracted adding 600ul of TRIzol reagent (Invitrogen, ThermoFisher) to the beads using manufacturers protocol.

Statistical analysis

Student's *t*-test was used for statistical analysis and performed using GraphPad Prism. Significance was determine at $p < 0,05$. Data are represented as mean mean ± s.d. Figure legends show the number of independent biological replicates (n).

Data availability

Raw data for the RNA-seq are deposited to GEO (GSE144752). Raw data for proteomics experiments are deposited to PRIDE ProteomeXchange (PXD017475). The data and reagents that support the findings of this study are available from the corresponding author upon reasonable request. Source data is available for Figs. 1–6 and Supplementary Figs. 1–6.

Declarations

ACKNOWLEDGEMENTS

We thank Morten Frodin for providing reagents. We thank the rest of the Lund lab for contributing with helpful discussions. The Lund lab is supported by grants from the Danish Council for Independent Research (Sapere Aude program); the Novo Nordisk Foundation; the Lundbeck Foundation and the Danish Cancer Society.

AUTHOR CONTRIBUTION

M.M. and A.H.L designed the experiments and analysed the data. M.M wrote the manuscript and all the coauthors gave comments and input. M.M., M.L., F.S.A, B.M. and S.T. conducted experimens. F.S.A analysed the RNA-seq data. M.L. performed the mass spectrometry experiments and analysis with help from L.M.H and J.S.A. N.R. and A.J.S.analysis *MIR31HG* expression in THCA and CRC from TCGA public available data.

CONFLICT OF INTEREST

None to declare

References

Acosta JC, Banito A, Wuestefeld T, Georgilis A, Janich P, Morton JP, Athineos D, Kang TW, Lasitschka F, Andrulis M, Pascual G, Morris KJ, Khan S, Jin H, Dharmalingam G, Snijders AP, Carroll T, Capper D, Pritchard C, Inman GJ et al. (2013) A complex secretory program orchestrated by the inflammasome controls paracrine senescence. Nature cell biology 15: 978-90

Acosta JC, O'Loghlen A, Banito A, Guijarro MV, Augert A, Raguz S, Fumagalli M, Da Costa M, Brown C, Popov N, Takatsu Y, Melamed J, d'Adda di Fagagna F, Bernard D, Hernando E, Gil J (2008) Chemokine signaling via the CXCR2 receptor reinforces senescence. Cell 133: 1006-18

Baker DJ, Wijshake T, Tchkonia T, LeBrasseur NK, Childs BG, van de Sluis B, Kirkland JL, van Deursen JM (2011) Clearance of p16Ink4a-positive senescent cells delays ageing-associated disorders. Nature 479: 232-6

Beiter T, Hoene M, Prenzler F, Mooren FC, Steinacker JM, Weigert C, Niess AM, Munz B (2015) Exercise, skeletal muscle and inflammation: ARE-binding proteins as key regulators in inflammatory and adaptive

networks. Exerc Immunol Rev 21: 42-57

Braig M, Lee S, Loddenkemper C, Rudolph C, Peters AH, Schlegelberger B, Stein H, Dorken B, Jenuwein T, Schmitt CA (2005) Oncogene-induced senescence as an initial barrier in lymphoma development. Nature 436: 660-5

Casella G, Munk R, Kim KM, Piao Y, De S, Abdelmohsen K, Gorospe M (2019) Transcriptome signature of cellular senescence. Nucleic acids research 47: 7294-7305

Chen Z, Trotman LC, Shaffer D, Lin HK, Dotan ZA, Niki M, Koutcher JA, Scher HI, Ludwig T, Gerald W, Cordon-Cardo C, Pandolfi PP (2005) Crucial role of p53-dependent cellular senescence in suppression of Pten-deficient tumorigenesis. Nature 436: 725-30

Chien Y, Scuoppo C, Wang X, Fang X, Balgley B, Bolden JE, Premsrirut P, Luo W, Chicas A, Lee CS, Kogan SC, Lowe SW (2011) Control of the senescence-associated secretory phenotype by NF-kappaB promotes senescence and enhances chemosensitivity. Genes & development 25: 2125-36

Christoffersen NR, Shalgi R, Frankel LB, Leucci E, Lees M, Klausen M, Pilpel Y, Nielsen FC, Oren M, Lund AH (2010) p53-independent upregulation of miR-34a during oncogene-induced senescence represses MYC. Cell death and differentiation 17: 236-45

Coppe JP, Desprez PY, Krtolica A, Campisi J (2010) The senescence-associated secretory phenotype: the dark side of tumor suppression. Annual review of pathology 5: 99-118

Coppe JP, Patil CK, Rodier F, Sun Y, Munoz DP, Goldstein J, Nelson PS, Desprez PY, Campisi J (2008) Senescence-associated secretory phenotypes reveal cell-nonautonomous functions of oncogenic RAS and the p53 tumor suppressor. PLoS biology 6: 2853-68

Cox J, Mann M (2008) MaxQuant enables high peptide identification rates, individualized p.p.b.-range mass accuracies and proteome-wide protein quantification. Nat Biotechnol 26: 1367-72

Daniotti M, Oggionni M, Ranzani T, Vallacchi V, Campi V, Di Stasi D, Torre GD, Perrone F, Luoni C, Suardi S, Frattini M, Pilotti S, Anichini A, Tragni G, Parmiani G, Pierotti MA, Rodolfo M (2004) BRAF alterations are associated with complex mutational profiles in malignant melanoma. Oncogene 23: 5968-77

Davies H, Bignell GR, Cox C, Stephens P, Edkins S, Clegg S, Teague J, Woffendin H, Garnett MJ, Bottomley W, Davis N, Dicks E, Ewing R, Floyd Y, Gray K, Hall S, Hawes R, Hughes J, Kosmidou V, Menzies A et al. (2002) Mutations of the BRAF gene in human cancer. Nature 417: 949-54

Demaria M, Ohtani N, Youssef SA, Rodier F, Toussaint W, Mitchell JR, Laberge RM, Vijg J, Van Steeg H, Dolle ME, Hoeijmakers JH, de Bruin A, Hara E, Campisi J (2014) An essential role for senescent cells in optimal wound healing through secretion of PDGF-AA. Developmental cell 31: 722-33

Dobin A, Davis CA, Schlesinger F, Drenkow J, Zaleski C, Jha S, Batut P, Chaisson M, Gingeras TR (2013) STAR: ultrafast universal RNA-seq aligner. Bioinformatics 29: 15-21

Dominguez D, Freese P, Alexis MS, Su A, Hochman M, Palden T, Bazile C, Lambert NJ, Van Nostrand EL, Pratt GA, Yeo GW, Graveley BR, Burge CB (2018) Sequence, Structure, and Context Preferences of Human RNA Binding Proteins. Molecular cell 70: 854-867 e9

Eide PW, Eilertsen IA, Sveen A, Lothe RA (2019) Long noncoding RNA MIR31HG is a bona fide prognostic marker with colorectal cancer cell-intrinsic properties. Int J Cancer 144: 2843-2853

El-Naggar AM, Veinotte CJ, Cheng H, Grunewald TG, Negri GL, Somasekharan SP, Corkery DP, Tirode F, Mathers J, Khan D, Kyle AH, Baker JH, LePard NE, McKinney S, Hajee S, Bosiljcic M, Leprivier G, Tognon CE, Minchinton AI, Bennewith KL et al. (2015) Translational Activation of HIF1alpha by YB-1 Promotes Sarcoma Metastasis. Cancer Cell 27: 682-97

Evdokimova V, Ruzanov P, Anglesio MS, Sorokin AV, Ovchinnikov LP, Buckley J, Triche TJ, Sonenberg N, Sorensen PH (2006) Akt-mediated YB-1 phosphorylation activates translation of silent mRNA species. Mol Cell Biol 26: 277-92

Evdokimova V, Ruzanov P, Imataka H, Raught B, Svitkin Y, Ovchinnikov LP, Sonenberg N (2001) The major mRNA-associated protein YB-1 is a potent 5' cap-dependent mRNA stabilizer. The EMBO journal 20: 5491-502

Evdokimova V, Tognon C, Ng T, Ruzanov P, Melnyk N, Fink D, Sorokin A, Ovchinnikov LP, Davicioni E, Triche TJ, Sorensen PH (2009) Translational activation of snail1 and other developmentally regulated transcription factors by YB-1 promotes an epithelial-mesenchymal transition. Cancer Cell 15: 402-15

Farr JN, Xu M, Weivoda MM, Monroe DG, Fraser DG, Onken JL, Negley BA, Sfeir JG, Ogrodnik MB, Hachfeld CM, LeBrasseur NK, Drake MT, Pignolo RJ, Pirtskhalava T, Tchkonia T, Oursler MJ, Kirkland JL, Khosla S (2017) Targeting cellular senescence prevents age-related bone loss in mice. Nat Med 23: 1072-1079

Freund A, Patil CK, Campisi J (2011) p38MAPK is a novel DNA damage response-independent regulator of the senescence-associated secretory phenotype. The EMBO journal 30: 1536-48

Georgilis A, Klotz S, Hanley CJ, Herranz N, Weirich B, Morancho B, Leote AC, D'Artista L, Gallage S, Seehawer M, Carroll T, Dharmalingam G, Wee KB, Mellone M, Pombo J, Heide D, Guccione E, Arribas J, Barbosa-Morais NL, Heikenwalder M et al. (2018) PTBP1-Mediated Alternative Splicing Regulates the Inflammatory Secretome and the Pro-tumorigenic Effects of Senescent Cells. Cancer Cell 34: 85-102 e9

Goldman M, Craft B, Hastie M, Repečka K, McDade F, Kamath A, Banerjee A, Luo Y, Rogers D, Brooks AN, Zhu J, Haussler D (2019) The UCSC Xena platform for public and private cancer genomics data visualization and interpretation. bioRxiv: 326470

Hayflick L (1965) The Limited in Vitro Lifetime of Human Diploid Cell Strains. Experimental cell research 37: 614-36

Hernandez-Segura A, de Jong TV, Melov S, Guryev V, Campisi J, Demaria M (2017) Unmasking Transcriptional Heterogeneity in Senescent Cells. Curr Biol 27: 2652-2660 e4

Herranz N, Gallage S, Mellone M, Wuestefeld T, Klotz S, Hanley CJ, Raguz S, Acosta JC, Innes AJ, Banito A, Georgilis A, Montoya A, Wolter K, Dharmalingam G, Faull P, Carroll T, Martinez-Barbera JP, Cutillas P, Reisinger F, Heikenwalder M et al. (2015) mTOR regulates MAPKAPK2 translation to control the senescence-associated secretory phenotype. Nature cell biology 17: 1205-17

Hoare M, Ito Y, Kang TW, Weekes MP, Matheson NJ, Patten DA, Shetty S, Parry AJ, Menon S, Salama R, Antrobus R, Tomimatsu K, Howat W, Lehner PJ, Zender L, Narita M (2016) NOTCH1 mediates a switch between two distinct secretomes during senescence. Nature cell biology 18: 979-92

Iannello A, Thompson TW, Ardolino M, Lowe SW, Raulet DH (2013) p53-dependent chemokine production by senescent tumor cells supports NKG2D-dependent tumor elimination by natural killer cells. The Journal of experimental medicine 210: 2057-69

Jeyapalan JC, Ferreira M, Sedivy JM, Herbig U (2007) Accumulation of senescent cells in mitotic tissue of aging primates. Mechanisms of ageing and development 128: 36-44

Jin C, Jia L, Huang Y, Zheng Y, Du N, Liu Y, Zhou Y (2016) Inhibition of lncRNA MIR31HG Promotes Osteogenic Differentiation of Human Adipose-Derived Stem Cells. Stem Cells 34: 2707-2720

Kang C, Xu Q, Martin TD, Li MZ, Demaria M, Aron L, Lu T, Yankner BA, Campisi J, Elledge SJ (2015) The DNA damage response induces inflammation and senescence by inhibiting autophagy of GATA4. Science 349: aaa5612

Krtolica A, Parrinello S, Lockett S, Desprez PY, Campisi J (2001) Senescent fibroblasts promote epithelial cell growth and tumorigenesis: a link between cancer and aging. Proceedings of the National Academy of Sciences of the United States of America 98: 12072-7

Kuilman T, Michaloglou C, Mooi WJ, Peeper DS (2010) The essence of senescence. Genes & development 24: 2463-79

Kuilman T, Michaloglou C, Vredeveld LC, Douma S, van Doorn R, Desmet CJ, Aarden LA, Mooi WJ, Peeper DS (2008) Oncogene-induced senescence relayed by an interleukin-dependent inflammatory network. Cell 133: 1019-31

Kwon E, Todorova K, Wang J, Horos R, Lee KK, Neel VA, Negri GL, Sorensen PH, Lee SW, Hentze MW, Mandinova A (2018) The RNA-binding protein YBX1 regulates epidermal progenitors at a posttranscriptional level. Nature communications 9: 1734

Laberge RM, Sun Y, Orjalo AV, Patil CK, Freund A, Zhou L, Curran SC, Davalos AR, Wilson-Edell KA, Liu S, Limbad C, Demaria M, Li P, Hubbard GB, Ikeno Y, Javors M, Desprez PY, Benz CC, Kapahi P, Nelson PS et al. (2015) MTOR regulates the pro-tumorigenic senescence-associated secretory phenotype by promoting IL1A translation. Nature cell biology 17: 1049-61

Li D, Liu X, Zhou J, Hu J, Zhang D, Liu J, Qiao Y, Zhan Q (2017) Long noncoding RNA HULC modulates the phosphorylation of YB-1 through serving as a scaffold of extracellular signal-regulated kinase and YB-1 to enhance hepatocarcinogenesis. Hepatology 65: 1612-1627

Li L, van Breugel PC, Loayza-Puch F, Ugalde AP, Korkmaz G, Messika-Gold N, Han R, Lopes R, Barbera EP, Teunissen H, de Wit E, Soares RJ, Nielsen BS, Holmstrom K, Martinez-Herrera DJ, Huarte M, Louloupi A, Drost J, Elkon R, Agami R (2018) LncRNA-OIS1 regulates DPP4 activation to modulate senescence induced by RAS. Nucleic acids research 46: 4213-4227

Liao Y, Smyth GK, Shi W (2014) featureCounts: an efficient general purpose program for assigning sequence reads to genomic features. Bioinformatics 30: 923-30

Lo Piccolo L, Mochizuki H, Nagai Y (2019) The lncRNA hsromega regulates arginine dimethylation of human FUS to cause its proteasomal degradation in Drosophila. J Cell Sci 132

Love MI, Huber W, Anders S (2014) Moderated estimation of fold change and dispersion for RNA-seq data with DESeq2. Genome Biol 15: 550

Lyabin DN, Eliseeva IA, Ovchinnikov LP (2014) YB-1 protein: functions and regulation. Wiley Interdiscip Rev RNA 5: 95-110

Martin M (2011) Cutadapt Removes Adapter Sequences From High-Throughput Sequencing Reads. In EMBnetjournal,

Martin M, Hua L, Wang B, Wei H, Prabhu L, Hartley AV, Jiang G, Liu Y, Lu T (2017) Novel Serine 176 Phosphorylation of YBX1 Activates NF-kappaB in Colon Cancer. The Journal of biological chemistry 292: 3433-3444

Matsumoto S, Uchiumi T, Tanamachi H, Saito T, Yagi M, Takazaki S, Kanki T, Kang D (2012) Ribonucleoprotein Y-box-binding protein-1 regulates mitochondrial oxidative phosphorylation (OXPHOS) protein expression after serum stimulation through binding to OXPHOS mRNA. Biochem J 443: 573-84

Michaloglou C, Vredeveld LC, Soengas MS, Denoyelle C, Kuilman T, van der Horst CM, Majoor DM, Shay JW, Mooi WJ, Peeper DS (2005) BRAFE600-associated senescence-like cell cycle arrest of human naevi. Nature 436: 720-4

Montes M, Lund AH (2016) Emerging roles of lncRNAs in senescence. The FEBS journal

Montes M, Nielsen MM, Maglieri G, Jacobsen A, Hojfeldt J, Agrawal-Singh S, Hansen K, Helin K, van de Werken HJ, Pedersen JS, Lund AH (2015) The lncRNA MIR31HG regulates p16(INK4A) expression to modulate senescence. Nature communications 6: 6967

Munoz-Espin D, Canamero M, Maraver A, Gomez-Lopez G, Contreras J, Murillo-Cuesta S, Rodriguez-Baeza A, Varela-Nieto I, Ruberte J, Collado M, Serrano M (2013) Programmed cell senescence during mammalian embryonic development. Cell 155: 1104-18

Nekrasov MP, Ivshina MP, Chernov KG, Kovrigina EA, Evdokimova VM, Thomas AA, Hershey JW, Ovchinnikov LP (2003) The mRNA-binding protein YB-1 (p50) prevents association of the eukaryotic initiation factor eIF4G with mRNA and inhibits protein synthesis at the initiation stage. The Journal of biological chemistry 278: 13936-43

Orjalo AV, Bhaumik D, Gengler BK, Scott GK, Campisi J (2009) Cell surface-bound IL-1alpha is an upstream regulator of the senescence-associated IL-6/IL-8 cytokine network. Proceedings of the National Academy of Sciences of the United States of America 106: 17031-6

Ozes AR, Miller DF, Ozes ON, Fang F, Liu Y, Matei D, Huang T, Nephew KP (2016) NF-kappaB-HOTAIR axis links DNA damage response, chemoresistance and cellular senescence in ovarian cancer. Oncogene

Prabhu L, Hartley AV, Martin M, Warsame F, Sun E, Lu T (2015) Role of post-translational modification of the Y box binding protein 1 in human cancers. Genes Dis 2: 240-246

Prabhu L, Mundade R, Wang B, Wei H, Hartley AV, Martin M, McElyea K, Temm CJ, Sandusky G, Liu Y, Lu T (2015) Critical role of phosphorylation of serine 165 of YBX1 on the activation of NF-kappaB in colon cancer. Oncotarget 6: 29396-412

Pritchard CA, Samuels ML, Bosch E, McMahon M (1995) Conditionally oncogenic forms of the A-Raf and B-Raf protein kinases display different biological and biochemical properties in NIH 3T3 cells. Mol Cell Biol 15: 6430-42

Proud CG (2019) Phosphorylation and Signal Transduction Pathways in Translational Control. Cold Spring Harb Perspect Biol 11

Rapicavoli NA, Qu K, Zhang J, Mikhail M, Laberge RM, Chang HY (2013) A mammalian pseudogene lncRNA at the interface of inflammation and anti-inflammatory therapeutics. Elife 2: e00762

Salama R, Sadaie M, Hoare M, Narita M (2014) Cellular senescence and its effector programs. Genes & development 28: 99-114

Serrano M, Lin AW, McCurrach ME, Beach D, Lowe SW (1997) Oncogenic ras provokes premature cell senescence associated with accumulation of p53 and p16INK4a. Cell 88: 593-602

Shih JW, Chiang WF, Wu ATH, Wu MH, Wang LY, Yu YL, Hung YW, Wang WC, Chu CY, Hung CL, Changou CA, Yen Y, Kung HJ (2017) Long noncoding RNA LncHIFCAR/MIR31HG is a HIF-1alpha co-activator driving oral cancer progression. Nature communications 8: 15874

Skabkina OV, Lyabin DN, Skabkin MA, Ovchinnikov LP (2005) YB-1 autoregulates translation of its own mRNA at or prior to the step of 40S ribosomal subunit joining. Mol Cell Biol 25: 3317-23

Storer M, Mas A, Robert-Moreno A, Pecoraro M, Ortells MC, Di Giacomo V, Yosef R, Pilpel N, Krizhanovsky V, Sharpe J, Keyes WM (2013) Senescence is a developmental mechanism that contributes to embryonic growth and patterning. Cell 155: 1119-30

Stratford AL, Fry CJ, Desilets C, Davies AH, Cho YY, Li Y, Dong Z, Berquin IM, Roux PP, Dunn SE (2008) Y-box binding protein-1 serine 102 is a downstream target of p90 ribosomal S6 kinase in basal-like breast cancer cells. Breast Cancer Res 10: R99

Sutherland BW, Kucab J, Wu J, Lee C, Cheang MC, Yorida E, Turbin D, Dedhar S, Nelson C, Pollak M, Leighton Grimes H, Miller K, Badve S, Huntsman D, Blake-Gilks C, Chen M, Pallen CJ, Dunn SE (2005) Akt phosphorylates the Y-box binding protein 1 at Ser102 located in the cold shock domain and affects the anchorage-independent growth of breast cancer cells. Oncogene 24: 4281-92

Tasdemir N, Banito A, Roe JS, Alonso-Curbelo D, Camiolo M, Tschaharganeh DF, Huang CH, Aksoy O, Bolden JE, Chen CC, Fennell M, Thapar V, Chicas A, Vakoc CR, Lowe SW (2016) BRD4 Connects Enhancer Remodeling to Senescence Immune Surveillance. Cancer Discov 6: 612-29

Thomas PD, Campbell MJ, Kejariwal A, Mi H, Karlak B, Daverman R, Diemer K, Muruganujan A, Narechania A (2003) PANTHER: a library of protein families and subfamilies indexed by function. Genome Res 13: 2129-41

Ventura A, Kirsch DG, McLaughlin ME, Tuveson DA, Grimm J, Lintault L, Newman J, Reczek EE, Weissleder R, Jacks T (2007) Restoration of p53 function leads to tumour regression in vivo. Nature 445: 661-5

Wang P, Xue Y, Han Y, Lin L, Wu C, Xu S, Jiang Z, Xu J, Liu Q, Cao X (2014) The STAT3-binding long noncoding RNA lnc-DC controls human dendritic cell differentiation. Science 344: 310-3

Wang Z, Deng Z, Dahmane N, Tsai K, Wang P, Williams DR, Kossenkov AV, Showe LC, Zhang R, Huang Q, Conejo-Garcia JR, Lieberman PM (2015) Telomeric repeat-containing RNA (TERRA) constitutes a nucleoprotein component of extracellular inflammatory exosomes. Proceedings of the National Academy of Sciences of the United States of America 112: E6293-300

Wickham H (2016) ggplot2: Elegant Graphics for Data Analysis.

Wu CH, van Riggelen J, Yetil A, Fan AC, Bachireddy P, Felsher DW (2007) Cellular senescence is an important mechanism of tumor regression upon c-Myc inactivation. Proceedings of the National

Academy of Sciences of the United States of America 104: 13028-33

Xu M, Palmer AK, Ding H, Weivoda MM, Pirtskhalava T, White TA, Sepe A, Johnson KO, Stout MB, Giorgadze N, Jensen MD, LeBrasseur NK, Tchkonia T, Kirkland JL (2015) Targeting senescent cells enhances adipogenesis and metabolic function in old age. Elife 4: e12997

Xue W, Zender L, Miething C, Dickins RA, Hernando E, Krizhanovsky V, Cordon-Cardo C, Lowe SW (2007) Senescence and tumour clearance is triggered by p53 restoration in murine liver carcinomas. Nature 445: 656-60

Yang H, Liu P, Zhang J, Peng X, Lu Z, Yu S, Meng Y, Tong WM, Chen J (2016) Long noncoding RNA MIR31HG exhibits oncogenic property in pancreatic ductal adenocarcinoma and is negatively regulated by miR-193b. Oncogene 35: 3647-57

Yang Y, Wang L, Han X, Yang WL, Zhang M, Ma HL, Sun BF, Li A, Xia J, Chen J, Heng J, Wu B, Chen YS, Xu JW, Yang X, Yao H, Sun J, Lyu C, Wang HL, Huang Y et al. (2019) RNA 5-Methylcytosine Facilitates the Maternal-to-Zygotic Transition by Preventing Maternal mRNA Decay. Molecular cell 75: 1188-1202 e11

Yoon JH, Abdelmohsen K, Kim J, Yang X, Martindale JL, Tominaga-Yamanaka K, White EJ, Orjalo AV, Rinn JL, Kreft SG, Wilson GM, Gorospe M (2013) Scaffold function of long non-coding RNA HOTAIR in protein ubiquitination. Nature communications 4: 2939

Figures

FIGURE 1. *MIR31HG* knock-down decreases the induction of SASP components during OIS

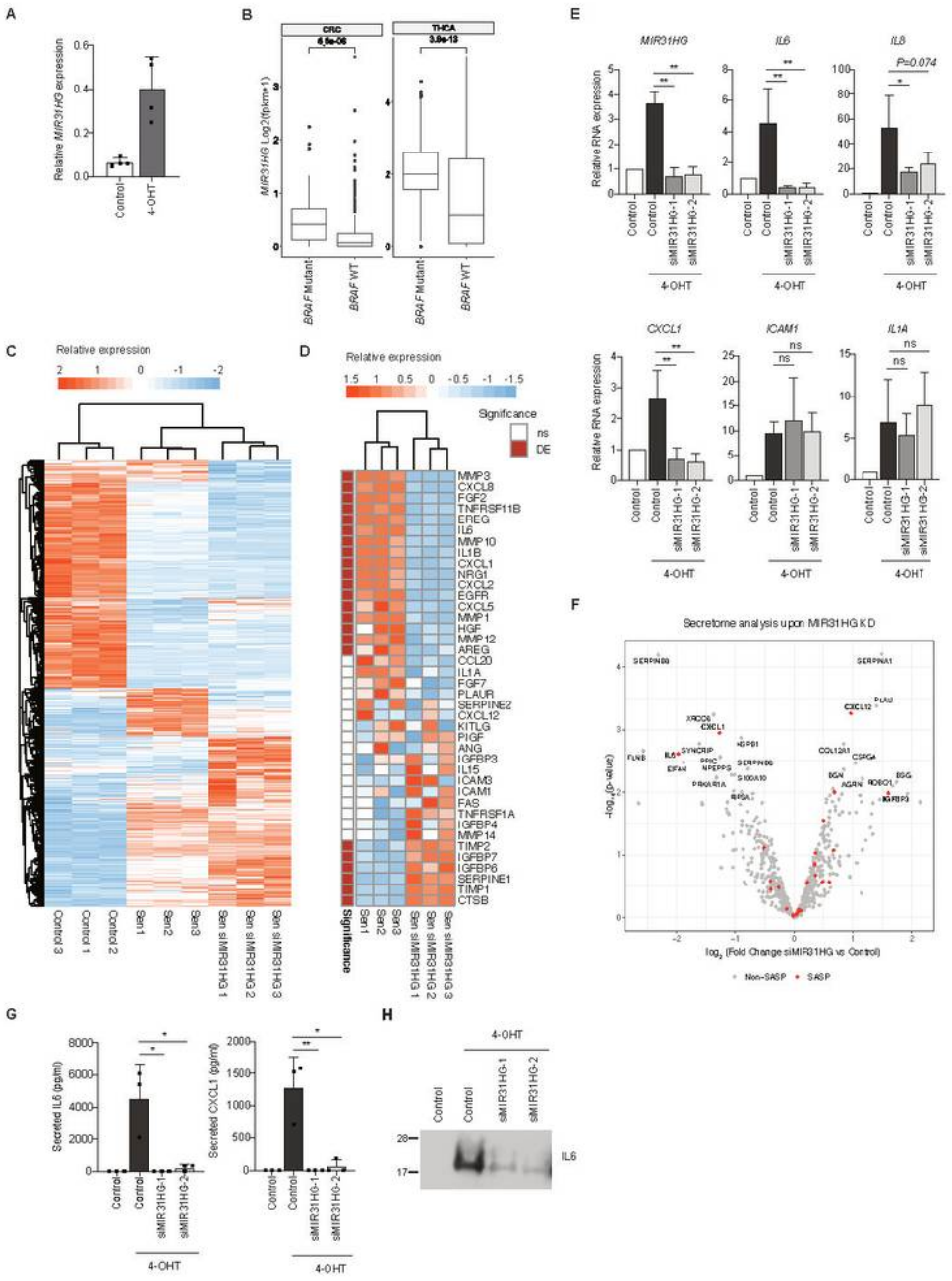

Figure 1

MIR31HG knock-down decreases the induction of SASP components during BRAF-induced senescence. (A) qRT–PCR analysis of MIR31HG expression normalized to housekeeping genes (HPRT1 and RPLP0) in BJ ER:BRAF cells were treated with ethanol (Control) or 1□M 4-OHT for 48h (n=4). (B) Box plot showing MIR31HG expression in log2(fpkm+1)units in Thyroid carcinoma (THCA) and colo-rectal carcinoma (CRC) comparing BRAF mutant and BRAF wild type tumors. Wilcoxon test was performed to compare the

expression differences in the BRAF mutant and BRAF wild type tumors. (C) BJ ER:BRAF cells (control or siMIR31HG) were treated with ethanol (Control 1-3) or 1□M 4-OHT for 48h (Sen 1-3 and Sen siMIR31HG 1-3) and further processed for RNA-seq (see materials and methods). The heat map shows relative expression of differentially expressed genes in the three conditions in triplicates. (D) The heat map shows relative expression in RPKMs of a subset of SASP genes previously defined(Coppe et al., 2010) from the data provide in (a), where differentially expressed genes ('DE', FDR < 0.01) are indicated in red, unchanged (non-significant, 'ns') in white;. (E) qRT–PCR analysis of selected components of the SASP normalized to housekeeping genes (HPRT1 and RPLP0) in BJ ER:BRAF cells transfected with the indicated siRNAs (Control or siMIR31HG1-2), treated with ethanol (Control) or 1□M 4-OHT for 48h. The graphs show results compared to control ethanol-treated set to 1 (n=4). (F) Mass spectrometry-based secretome analysis of senescent BJ ER:BRAF (1□M 4-OHT) treated with MIR31HG or control siRNA. The volcano plot shows differentially secreted proteins in MIR31HG knock-down senescent cells (Sen siMIR31HG) compared to control senescence cells (Sen) (-log10 pvalue along y-axis and log fold change along x-axis). Names are displayed for significantly changed proteins between secretomes (pval < 0.01) and SASP proteins are marked in red. (G) BJ ER:BRAF (Control or siMIR31HG1-2) were treated for 72h with ethanol (Control) or 1□M 4-OHT. The CM was then harvested and secreted CXCL1 and IL6 were measured by ELISA. The graph shows the pg/ml of secreted protein (n=3). (H) BJ ER:BRAF (Control or siMIR31HG1-2) were treated for 72h with 1□M 4-OHT. The CM was then harvested and proteins were precipitated using EtOH . IL6 protein expression was analysed by western blot. Molecular weight marker is shown in kDa (n=3). All statistical significances were calculated using two-tailed Student t-tests, **P < 0.01; *P < 0.05; ns, non-significant. All error bars represent mean ± s.d.

FIGURE 2 . The SASP of senescent *MIR31HG* knock-down cells induces senescence but not invasion in a non-autonomous manner

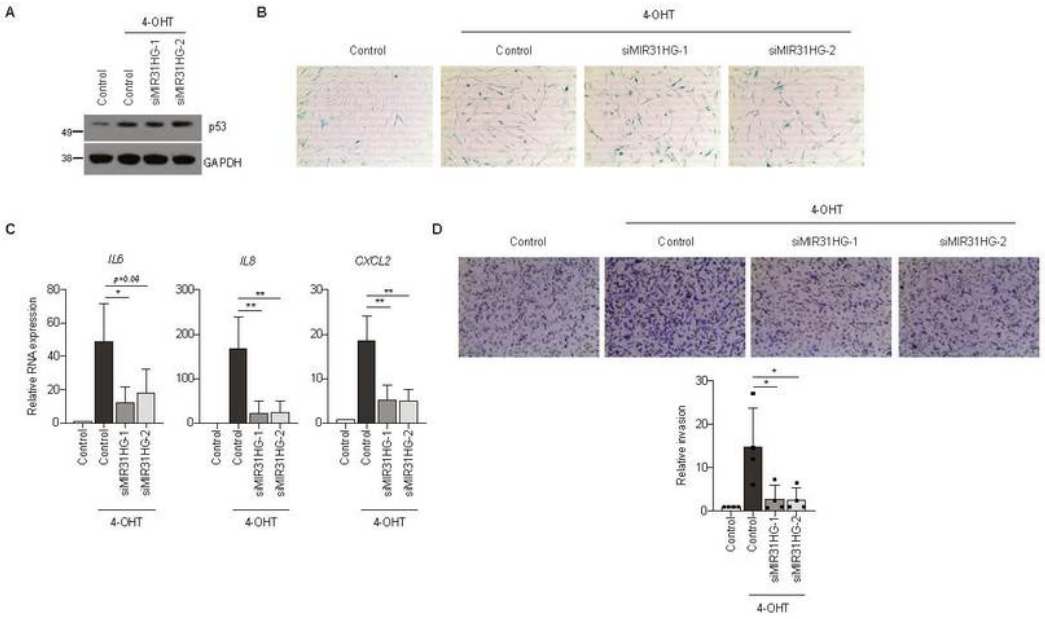

Figure 2

The SASP of senescent MIR31HG knock-down cells induces senescence but not invasion in a non-autonomous manner. (A) Wild type BJ cells were incubated for 72h with the CM collected from BJ ER:BRAF cells (Control or siMIR31HG1-2) treated with ethanol (Control) or 1□M 4-OHT for 72h. Whole cell extracts were analysed by western blot for p53 and GAPDH. Molecular weight marker is shown in kDa (n=3). (B) Representative images of □-galactosidase staining from the same condition as indicated in (a)

(C) qRT–PCR analysis of a subset of components of the SASP normalized to housekeeping genes (HPRT1 and RPLP0) in total RNA extracted from cells described in (a). The graph shows the RNA expression relative to control ethanol-treated cells set to 1 (n=4). (D) MDA-MB-231 cells were placed in the upper part of a transwell assay in contact with the CM collected from BJ ER:BRAF cells (Control or siMIR31HG) treated for 72h with ethanol (Control) or 1□M 4-OHT. After 24h cells invading the matrigel membrane were stained with crystal violet. Representative images are shown in the figure. Bottom panel, quantification of the invading cells relative to control ethanol-treated cells (n=3). All statistical significances were calculated using two-tailed Student t-tests, **P < 0.01; *P < 0.05. All error bars represent mean ± s.d.

FIGURE 3. *MIR31HG* knock-down decreases CEBPB protein levels and NFkB nuclear translocation

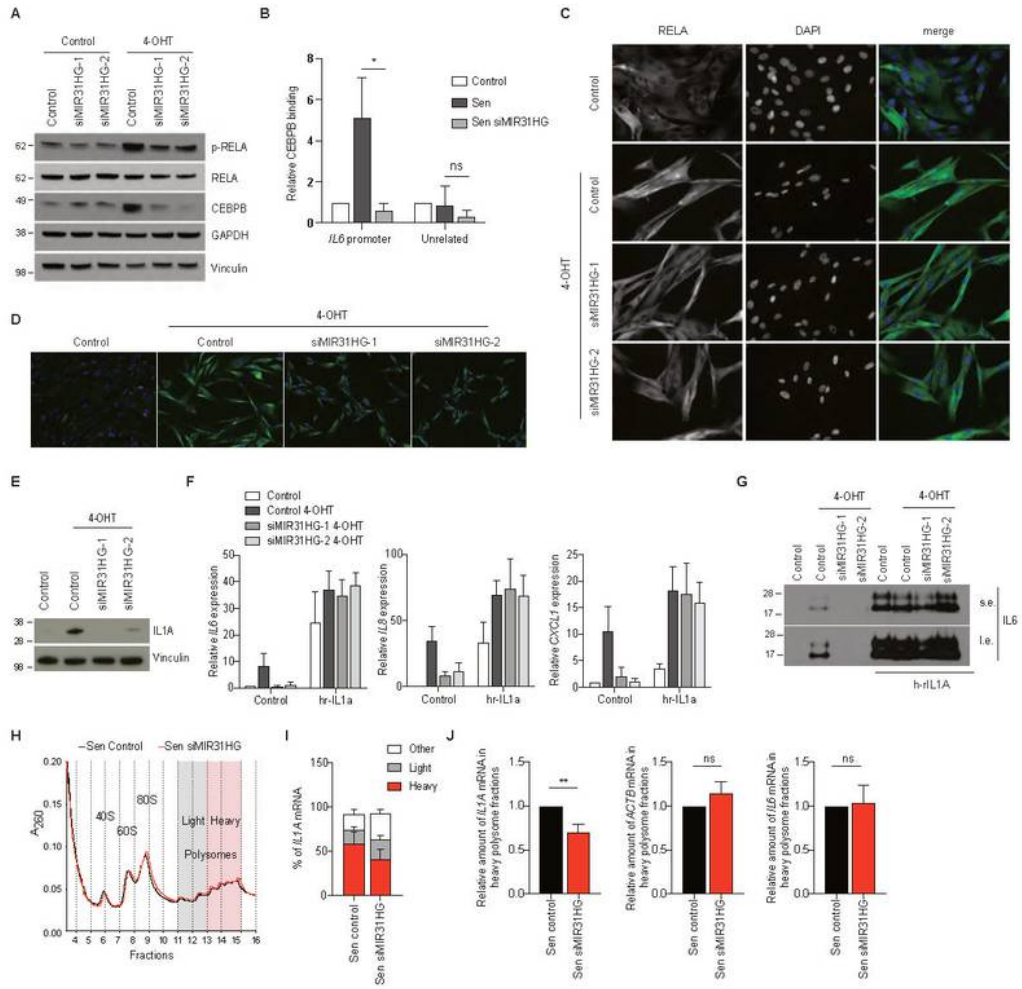

Figure 3

MIR31HG knock-down decreases IL1A translation. (A) BJ ER:BRAF cells (Control or siMIR31HG1-2) were treated with ethanol (Control) or 1□M 4-OHT for 72h. Whole cell extracts were analysed by western blot for p-RELA, RELA and CEBPB. Vinculin and GAPDH were used as loading controls. Molecular weight marker is shown in kDa (n=3). (B) Chromatin immunoprecipitation followed by qPCR for CEBPB binding to the IL6 promoter in BJ ER:BRAF cells (Control or siMIR31HG1) treated with ethanol (Control) or 1□M 4-OHT

for 48h. The graph shows the ratio of CEBPB to IgG binding normalized to the binding in control cells set as 1 (n=3). (C) BJ ER:BRAF cells (Control or siMIR31HG1-2) were treated with ethanol (Control) or 1□M 4-OHT for 72h and processed for immunofluorescence (see materials and methods). Representative images of RELA immunofluorescence and DAPI (4,6-diamidino-2-phenylindole) are shown in the figure (n-3). (D) BJ ER:BRAF cells (Control or siMIR31HG1-2) were treated with ethanol (Control) or 1□M 4-OHT for 72h and processed for immunofluorescence (see materials and methods). Representative merged images of IL1A and DAPI are shown in the figure (n=3). (E) BJ ER:BRAF cells (Control or siMIR31HG1-2) were treated with ethanol (Control) or 1□M 4-OHT for 72h. Whole cell extracts were analysed by western blot for IL1A protein levels. Vinculin is shown as loading control. Molecular weight marker is shown in kDa (n=3). (F) qRT-PCR analysis for the indicated SASP factors in BJ ER:BRAF cells transfected with the indicated siRNAs (Control or siMIR31HG1-2), treated with ethanol (Control) or 1□M 4-OHT for 48h, in the absence or presence of 10ng/ml of h-rIL1A for 2h before RNA extraction (n=3). (G) Western blot for IL6 from precipitated protein from the media in the conditions indicated in (f) in in the absence or presence of 10ng/ml of h-rIL1A for 24h before harvesting the CM (n=3). (s.e, short exposure, l.e, long exposure). (H) Polysome profile performed by sucrose gradient separation in BJ ER:BRAF control cells (Sen, black) or siMIR31HG cells (Sen siMIR31HG, red) treated with 1□M 4-OHT for 72h. Y axis shows the absorbance at 260nM and X axis shows the number of the fractions collected. Red area shows the heavy polysome fractions and grey area shows the light polysome fractions. One representative experiment is shown in the figure (n=3). (I) Distribution of the amount of IL1A mRNA in the heavy polysome (red) light polysome (grey) or other fractions (white) from the experiment in (g). (J) Relative amount of IL1A, IL6 and ACTB mRNA present in the heavy polysome fractions in the experiment described in (J). All statistical significances were calculated using two-tailed Student t-tests, **P < 0.01; ns, non-significant. All error bars represent mean ± s.d.

FIGURE 4. *MIR31HG* interacts with YBX1 and YBX1 knock-down phenocopies MIR31HG depletion

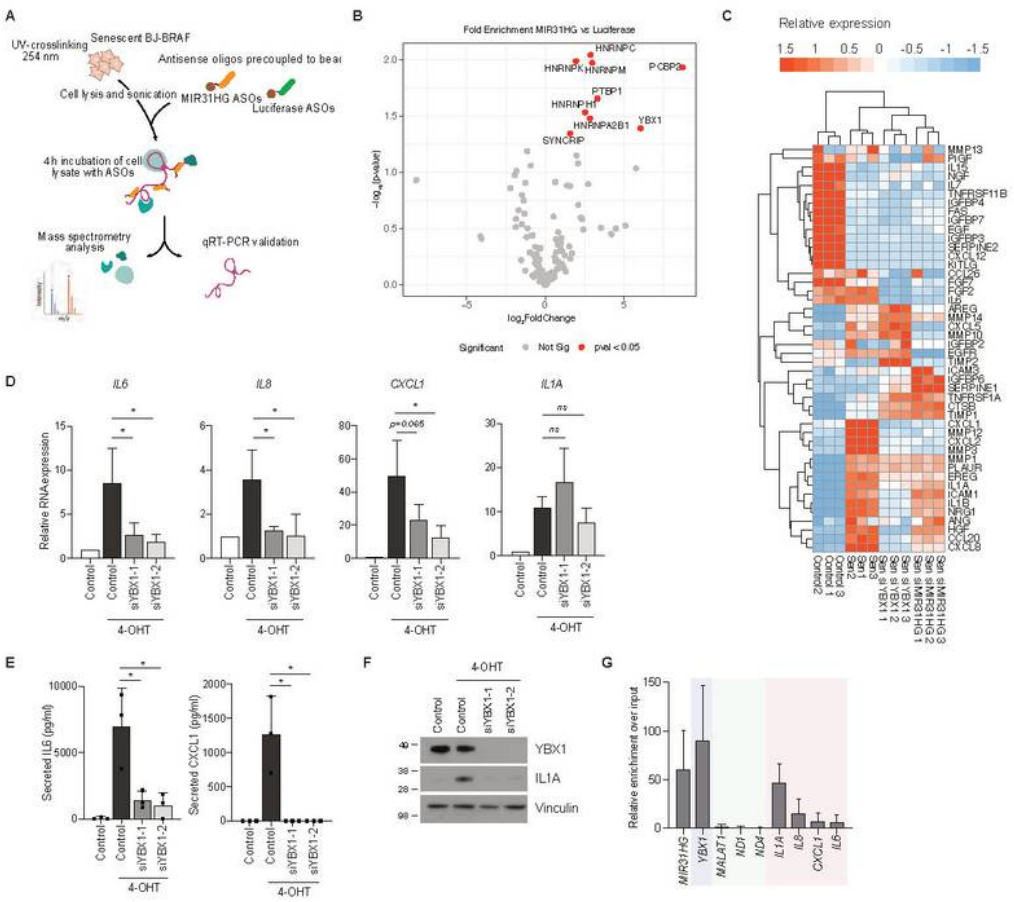

Figure 4

MIR31HG interacts with YBX1. (A) Schematic representation of the pull-down procedure. (B) Cellular extracts from BJ ER:BRAF (Control or siMIR31HG) treated with 1□M 4-OHT for 72h were incubated with antisense oligos, enriched proteins extracted and subjected to LC-MS analysis (see materials and methods). The volcano plot highlights proteins enriched in the MIR31HG pull down analysis compared to a luciferase control pull down. Marked in red are protein with pvalue < 0.05. (C) The heat map shows the

relative expression of significant differentially expressed genes in BJ ER:BRAF cells (control or siMIR31HG) treated with ethanol (Control1-3) or 1μM 4-OHT for 48h (Sen 1-3, Sen siMIR31HG 1-3, Sen YBX1-KD1-3) (D) qRT–PCR analysis of selected components of the SASP normalized to housekeeping genes (HPRT1 and RPLP0) in BJ ER:BRAF cells transfected with the indicated siRNAs (Control or siYBX1, 1-2), treated with ethanol (Control) or 1μM 4-OHT for 48h. The graph shows results compared to control ethanol-treated set to 1 (n=4). (E) BJ ER:BRAF (Control or siYBX1, 1-2) were treated for 72h with ethanol (Control) or 1μM 4-OHT. The CM was then harvested and secreted CXCL1 and IL6 were measured by ELISA. The graph shows the pg/ml of secreted protein (n=3). (F) BJ ER:BRAF cells (Control or siYBX1, 1-2) were treated with ethanol (Control) or 1μM 4-OHT for 72h. Whole cell extracts were analysed by western blot for IL1A protein levels. Vinculin is shown as loading control. Molecular weight marker is shown in kDa (n=3). (G) BJ ER:BRAF cells carrying a GFP-YBX1 were induced with 1μM 4-OHT for 72h and crosslinked and processed for RIP (see materials and methods) The graph shows YBX1 binding as positive control (blue), MALAT1, ND1 and ND4 binding as negative controls (green) and cytokines binding (pink). The results are shown as percentage of input relative to an empty GFP cell line treated in the same conditions (n=3). All statistical significances were calculated using two-tailed Student t-tests, **P < 0.01; *P < 0.05; ns, non-significant. All error bars represent mean ± s.d.

FIGURE 5. Phosphorylated YBX1 induces IL1A translation

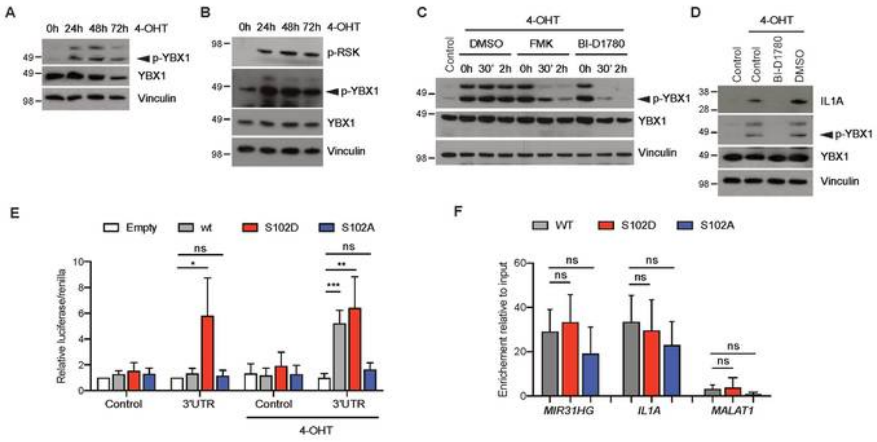

Figure 5

Phosphorylated YBX1 induces IL1A translation. (A) BJ ER:BRAF cells treated with 1□M 4-OHT for the indicated time were analysed by western blot for p-YBX1 (arrow) and total YBX1. Vinculin is used as loading control. Molecular weight marker is shown in kDa (n=2). (B) Western blot for pRSK1, RSK1, p-YBX1, total YBX1 and VCL in BJ ER:BRAF cells treated with 1□M 4-OHT for the indicated time. Molecular weight marker is shown in kDa (n=3). (C) BJ ER:BRAF cells untreated (control) or treated with 1□M 4-OHT

and the corresponding inhibitors at 1μM for the indicated time were analysed by western blot for p-YBX1, total YBX1. DMSO is used as vehicle control. Vinculin is used as loading control. Molecular weight marker is shown in kDa (n=3). (D) BJ ER:BRAF cells untreated (control) or treated with 1μM 4-OHT and the indicated inhibitor at 1μM for 72h were analysed by western blot for p-YBX1, total YBX1, IL1A and Vinculin. Molecular weight marker is shown in kDa (n>4). (E) BJ ER:BRAF cells expressing a doxycycline-induced empty, wild type, mutant S102A or mutant S102D versions of YBX1 were transfected with a siRNA against YBX1. 24h later cells were transfected with luciferase reporter constructs pGL3-promoter (control) or pGL3-promoter-3'UTR (3'UTR) containing the 3'UTR of IL1A mRNA and treated with ethanol (control) or with 1μM 4-OHT for 48h. The graph shows the the luciferase values normalized to renilla and relative to the empty cell line in the absence of 4-OHT set as 1 (n=4). (F) RIP analysis using a GFP-tagged version of WT YBX1, S102A mutant or S102D mutant in formaldehyde crosslinked cells induced with doxycycline and treated with 1μM 4-OHT for 72h. The graph shows YBX1 binding to MIR31HG, IL1A and MALAT as negative control. The results are shown as percentage of input relative to an empty GFP cell line treated in the same conditions (n=4). All statistical significances were calculated using two-tailed Student t-tests, ***P< 0.001; **P < 0.01; *P < 0.05; ns, non-significant. All error bars represent mean ± s.d.

FIGURE 6. *MIR31HG* knock-down in senescent cells reduces phosphorylation of cytoplasmic YBX1 inhibiting its interaction with RSK

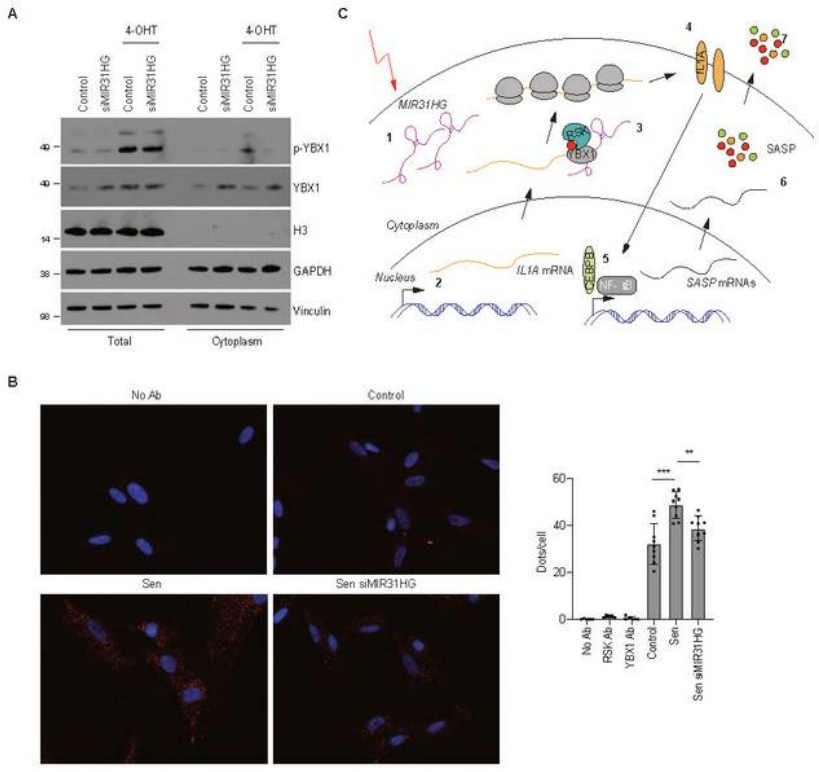

Figure 6

MIR31HG inhibits YBX1 interaction with its kinase RSK. (A) BJ ER:BRAF cells (Control or siMIR31HG1-2) were treated with ethanol (Control) or 1□M 4-OHT for 72h. After cellular fractionation p-YBX1 and YBX1in the total and cytoplasmic fractions were analysed by western blot. Vinculin and GAPDH were used as cytoplasmic controls and histone H3 as nuclear control (n=3). (B) BJ ER:BRAF cells (Control or siMIR31HG1) were treated with ethanol (Control) or 1□M 4-OHT for 72h. The cells were fixed and

processed for PLA (see materials and methods). PLA representative images showing the interaction (red dots) between YBX1 and RSK are shown in the figure (left). Quantification of the number of interactions (dots) per cell in the conditions indicated (right) in a representative experiment out of 4 independent replicates (n=4). Statistical significance was calculated using two-tailed Student t-tests, ***P< 0.001; **P < 0.01. Error bars represent mean ± s.d. (C) Scheme of the working model. 1) During OIS MIR31HG is induced and locates in the cytoplasm. 2) At the same time, transcription of IL1A mRNA is induced. 3) IL1A mRNA is exported to the cytoplasm where it interacts with YBX1. MIR31HG facilitates YBX1 interaction with the kinase RSK promoting its phosphorylation which in turns promotes IL1A translation. 4) IL1A signalling induces the transcription of other SASP mRNAs through CEBPB and NF-kB. 5) These RNAs will be translated in the cytoplasm and the SASP components will be secreted (6).

Supplementary Files

This is a list of supplementary files associated with this preprint. Click to download.

- SupplementaryFigures.pdf
- SupplementaryTable4.xlsx
- SupplementaryTable4.xlsx
- SupplementaryTable4.xlsx
- SupplementaryTable4.xlsx
- SupplementaryTable4.xlsx
- SupplementaryTable5.xlsx
- SupplementaryTable2.xlsx
- SupplementaryTable3.xlsx
- SupplementaryTable1.xlsx